LRRK2 modifies α-syn pathology and spread in mouse models and human neurons

Authors:

Gregor Bieri[1,2], Michel Brahic[1], Luc Bousset[3], Julien Couthouis[1], Nicholas Kramer[1,2], Rosanna Ma[1], Lisa Nakayama[1], Marie Monbureau[4,5], Erwin Defensor[4,5], Birgitt Schuele[6], Mehrdad Shamloo[4,5], Ronald Melki[3], Aaron D. Gitler[1,2]*.

1. Department of Genetics, Stanford University School of Medicine, Stanford, CA, USA
2. Stanford Neurosciences Graduate Program, Stanford University School of Medicine, Stanford, CA, USA
3. Institut François Jacob, MIRCen, CEA and Laboratory of Neurodegenerative Diseases, CNRS, Fontenay-aux-Roses, France
4. Stanford Behavioral and Functional Neuroscience Laboratory, Stanford University, Stanford, CA, USA
5. Department of Neurosurgery, Stanford University School of Medicine, Stanford, CA, USA
6. Department of Pathology, Stanford University School of Medicine, CA, USA

***Corresponding Author:**

Aaron D. Gitler, Ph.D.
Department of Genetics
Stanford University School of Medicine
300 Pasteur Drive
M322 Alway Building
Stanford, CA 94305-5120

Email: agitler@stanford.edu
Tel: (650) 725-6991
Fax: (650) 725-1534

Abstract:

Progressive aggregation of the protein alpha-synuclein (α-syn) and loss of dopaminergic neurons in the substantia nigra pars compacta (SNpc) are key histopathological hallmarks of Parkinson's disease (PD). Accruing evidence suggests that α-syn pathology can propagate through neuronal circuits in the brain, contributing to the progressive nature of the disease. Thus, it is therapeutically pertinent to identify modifiers of α-syn transmission and aggregation as potential targets to slow down disease progression. A growing number of genetic mutations and risk factors have been identified in studies of both familial and sporadic forms of PD. However, how these genes affect α-syn aggregation and pathological spread, and whether they can be targeted for therapeutic interventions, remains unclear. We performed a targeted genetic screen of risk genes associated with PD and parkinsonism for modifiers of α-syn aggregation, using an α-syn preformed-fibril (PFF) induction assay. We found that decreased expression of Lrrk2 and Gba modulated α-syn aggregation in mouse primary neurons. Conversely, α-syn aggregation increased in primary neurons from transgenic mice expressing the PD-linked LRRK2 G2019S mutation. *In vivo*, we investigated α-syn spreading in a LRRK2 G2019S transgenic mouse model and observed acceleration of α-syn aggregation and degeneration of dopaminergic neurons in the SNpc. Furthermore, LRRK2 G2019S transgenic mice displayed more pronounced degeneration-associated neuroinflammation and exacerbated behavioral deficits. To validate our findings in a human context, we established a human α-syn transmission model using induced pluripotent stem cell (iPS)-derived neurons (iNs). Recombinant human α-syn PFFs triggered aggregation of endogenous α-syn in a time-dependent manner in human iNs. In isogenic lines of human iNs, the G2019S mutation enhanced α-syn aggregation, whereas loss of LRRK2 decreased aggregation. Collectively, these findings establish a strong interaction between the PD risk gene LRRK2 and α-syn transmission across mouse and human models. Since clinical trials of LRRK2 inhibitors in PD are currently underway, our findings raise the possibility that these may be effective in PD broadly, not just in the cases caused by LRRK2 mutations.

Key words:
Parkinson's disease, alpha-synuclein, pre-formed fibrils (PFF), LRRK2, GBA, prion-like propagation, genetic interaction.

Introduction:

Parkinson's disease (PD) is characterized by a progressive loss of midbrain dopaminergic neurons in the substantia nigra pars compacta (SNpc), resulting in motor symptoms, including rigidity, postural instability, tremor, and movement defects [24, 32]. A defining pathological feature of PD is the presence of intracellular protein aggregates termed Lewy bodies (LB), whose major component is the protein alpha-synuclein (α-syn) [17, 18, 23, 32]. To date, a growing number of dominant and recessive genetic mutations, as well as genetic risk factors, have been identified in families with a high prevalence of PD (fPD), accounting for approximately 5-10% of all PD cases. Further, genome-wide association studies (GWAS) have identified additional genomic loci and candidate genes conferring risk for PD [10]. Rare mutations in *SNCA*, the gene encoding α-syn, as well as duplications and triplications of the locus haven been linked to PD - establishing a direct genetic link between PD and α-syn [4, 11, 33, 34, 47, 51, 61].

α-Syn exhibits certain 'prion-like' properties, such as the ability to spread through the brain from cell to cell and trigger aggregation of endogenous α-syn [31]. It has been suggested that in human PD brains, α-syn pathology is present in the brainstem prior to the onset of motor dysfunction, progressively extending to interconnected brain areas such as the SNpc and eventually the neocortex [7, 8]. A variety of *in vitro* and *in vivo* models have been developed, illuminating the cell-to-cell transmission properties of α-syn pathology. In particular, α-syn preformed-fibril (PFF) based rodent models have emerged as a powerful tool to investigate uptake, transport, aggregation and neurodegeneration [9, 20, 38, 57]. Indeed, local injection of α-syn fibrils into the brains of wild type (WT) mice leads to aggregation of endogenous α-syn within neurons of connected regions distant from the injection site [38]. Together, this emerging body of work indicates that α-syn can be taken up by neurons and transmitted to other neurons in interconnected brain areas, where it can trigger aggregation.

Although considerable progress has been made in support of the progressive nature of α-syn pathology, the mechanism underlying the spread of α-syn aggregates between neurons - and the effect of PD-causing mutations on this process - remains poorly understood [6]. We wondered whether some of the genes that contribute to PD do so by converging on α-syn aggregation and spread [1]. We performed a series of α-syn PFF-based experiments investigating the effect of a selection of PD-associated risk genes on transmission and aggregation of α-syn pathology in mouse primary neurons, a PFF-based mouse model of PD, and human induced pluripotent stem cell (iPS)-derived neurons from PD patients. In a targeted knock down (KD) and overexpression screen, LRRK2 and GBA, two of the most common genetic risk factors for PD, modulated the extent of α-syn aggregation in mouse primary neurons [29]. *In vivo*, we used an intra-striatal PFF delivery mouse model of PD and observed that α-syn aggregation was exacerbated in transgenic mice carrying the LRRK2 G2019S variant, the most common genetic cause of fPD. In addition to accelerated degeneration of tyrosine hydroxylase (TH)-positive neurons in the SNpc, LRRK2 G2019S transgenic mice also developed more pronounced neuroinflammation and behavioral deficits. To translate our findings in a human context, we employed an approach to rapidly differentiate human iPS cells into induced neurons (iNs) [63] and developed a human *in vitro* model of α-syn transmission and aggregation. Recombinant human PFFs were rapidly internalized in human iNs and induced aggregation of endogenous α-syn. Furthermore, using iPS-derived neurons from fPD patients carrying the LRRK2 G2019S mutation, we observed an increase in α-syn aggregation in human iNs. Conversely, α-syn aggregation was reduced in isogenic LRRK2 knock out (KO) iNs. Collectively, these findings validate our aggregation-based targeted screening approach and identify a strong genetic interaction between LRRK2 and α-syn in both mouse and

human PFF-based models of aggregation and spreading. These results have potential implications for clinical trials of LRRK2 inhibitors that are currently underway.

Materials and Methods:

Animals

Mouse husbandry and procedures were performed in accordance with institutional guidelines and approved by the Stanford Administrative Panel on Animal Care (APLAC). Heterozygous human LRRK2 G2019S BAC transgenic mice (The Jackson Laboratory, cat# 018785) were maintained on a C57BL/6 background (The Jackson Laboratory, cat# 000664). LRRK2 G2019S mice and wild-type litter-mates were used for *in vivo* experiments. C57BL/6 mice, LRRK2 G2019S BAC mice and *CAG–Cas9* transgenic mice (Jackson Laboratory cat# 024858) were used for time-mating and primary neuron cultures.

Stereotaxic injections

Stereotaxic injections were performed on 8-12 week old adult mice. Animals were placed in a stereotaxic frame and anesthetized with 2% isoflurane (2L/min oxygen flow rate) delivered through an anesthesia nose cone. Ophthalmic eye ointment was applied to prevent desiccation of the cornea during surgery. The area around the incision was trimmed and disinfected. PFF or vehicle solutions were injected unilaterally or bilaterally into the dorsal striatum using the following coordinates (from bregma): anterior = +0.4mm, lateral = +/-1.85mm from midline, depth = -2.7mm (from dura). Mice were injected with sonicated PFFs or PBS vehicle control. PFFs were sonicated prior to injection. Per hemisphere, 1µl volume was injected at a rate of 100nl/min using a 5µl Hamilton syringe with a 32G needle. To limit reflux along the injection track, the needle was maintained in situ for five minutes, before being slowly retrieved. Each mouse was injected subcutaneously with analgesics and monitored during recovery.

Behavioral testing

Animals underwent a series of behavioral testing up to 6 months post-injection. All behavioral assays were conducted by an investigator blinded to the genotype and treatment condition. Mice were habituated to the behavioral testing room and investigator prior to the behavioral testing. All testing equipment was cleaned with Virkon and 70% ethanol between animals.

-*Rotarod* was used to assess motor learning and coordination. To acclimate them to the Rotarod apparatus, mice were trained on 3 consecutive days for 5min at constant speed of 10rpm. For the testing, thee speed was gradually increased from 4-40rmp over the course of 5min. Latency to fall was measured for 3 trials/day on 3 consecutive days. The rod and chambers were wiped with 70% ethanol between trials.

-*Pole test* was used to measure motor coordination and function. Mice were placed on a vertical pole and the latency to descend was measured for 3 trials.

-*Wire hang test* was used to test motor function and deficit. Mice were placed on a grid that was then inverted. The latency to fall was recorded for two consecutive trials.

-*Open Field* was used to measure spontaneous activity, locomotion and anxiety. Animals are placed in the square open field arena (76cm x 76cm x 50cm) and allowed to freely move while being recorded by the automated tracking system (Ethovision) for up to 10 minutes. Distance traveled, number of entries and time spent in the center and periphery was automatically assessed.

Tissue processing
Mice were anesthetized with isoflurane and transcardially perfused with 0.9% saline. Brains were dissected and fixed in 4% paraformaldehyde (PFA) pH 7.4, at 4°C for 48 hours. Brains were then stored in 30% sucrose in 1x PBS at 4°C. For unilateral injection experiments, the whole brain was fixed in PFA. For bilateral injection experiments, one hemibrain was fixed in PFA whereas the other hemibrain was sub-dissected, snap frozen in liquid nitrogen and stored at -80°C for biochemical analysis. PFA fixed brains were sectioned at 35µm (coronal sections) with a cryo-microtome (Leica) and stored in cryoprotective medium (30% glycerol, 30% ethylene glycol) at -20°C.

Immunohistochemistry
Tissue processing and immunohistochemistry was performed on free-floating sections according to standard published techniques. 1:4 to 1:12 series coronal sections were used for all histological experiments. Sections were rinsed 3 times in TBST, pre-treated with 0.6% H_2O_2 and 0.1% Triton X-100 (Sigma-Aldrich) and blocked in 5% goat serum in TBST. The following primary antibodies were used: NeuN (1:1000, Millipore, Cat# MAB377), Tyrosine Hydroxylase (TH; 1:1000; Pel-Freez, cat# P40101-0), α-syn pSer129 (81A; 1:5000, Covance/BioLegend cat# MMS-5091); α-syn pSer129 (1:3000; Abcam cat# 51253), LRRK2 (1:1000; NeuroMAP cat# 75-253) , p62 (1:1000; Proteintech cat# 18420-AP), GFAP (1:1000; Dako cat# Z0334), Iba1 (1:1000; Wako cat# 019-19741), CD68 (1:500; AbD Serotec cat# MCA1957GA), C1q (1:1000; Abcam cat# ab182451). After overnight incubation at 4°C, the primary antibody staining was revealed using biotinylated secondary antibodies, ABC kit (Vector Laboratories) and 3,3'-diaminobenzidine tetrahydrochloride (DAB, Sigma-Aldrich). Fluorescently labeled secondary antibodies were used for fluorescent and confocal microscopy. Sections were mounted on Superfrost Plus slides (Fisher Scientific) and coverslipped using Entellan (for DAB staining) or ProlongDiamond antifiade mountant (for fluorescent immunostaining). Imaging and unbiased stereological estimations of TH and pSer129-positive cells were performed by investigators blinded to genotype and experimental conditions. Per animal 8-10 SNpc sections were used for TH-neuron analysis. 3-5 sections per animal and brain region were used for all other immunostainings.

Western blotting
Mouse brain tissue was subdissected, snap frozen and stored at -80ºC until further use. *In vitro*, iPS cells and neurons were washes with ice-cold PBS prior to lysis. Cells or tissue were lysed on ice in 1x RIPA lysis buffer or sequentially in 1% Triton X followed by 2% SDS lysis buffer supplemented with 1x Halt protease and phosphatase Inhibitor Cocktail (Thermo Fisher Scientific cat# 78429, 78426). [56]. Crude RIPA lysates were centrifuged at 15,000 *g* for 10 min at 4°C to remove cellular debris. TritonX-lysates were centrifuged at approximately 15,000g for 10min at 4°C. The pellet was resuspended and sonicated in 2% SDS lysis buffer. Clarified lysates were quantified with a Pierce BCA protein assay (Thermo Fisher Scientific cat# 23225). Cell lysates were mixed with 4x NuPage LDS loading buffer or 4x Laemmli buffer and equal amounts of protein were subjected to SDS–PAGE, transferred to PVDF or nitrocellulose membranes. For the detection of total α-syn and α-syn pSer129, PVDF membranes were fixed with 0.4% PFA for 30 minutes at room temperature [35]. Membranes were blocked with 5% milk or 5% BSA in Tris-Buffered Saline with 0.1% Tween (TBST) and immunoblotted according to standard protocols. The following antibodies were used: ACTB (clone C4; 1:5000; Millipore cat#), GAPDH (1:5,000, Sigma cat# G8795), α-synuclein (1:1000, Novus Biologicals cat# NBP-92694), α-syn pSer129 (Abcam cat# 51253, 1:5000), LRRK2 (1:1000, Abcam cat# ab133474), LRRK2 phosphoS1292 (1:1000 Abcam cat# ab203181), GBA (1:1000; Novus Biologicals cat# NBP1-32271), RAB10

phospho T73 (1:1000, Abcam cat# ab230261), Synaptophysin 1 (SYSY cat# 101 002), PSD95 (1:5000; Abcam cat# ab18258), Homer1 (SYSY cat# 160 003). Following incubation at 4°C overnight, horseradish peroxidase-conjugated secondary antibodies and an ECL kit (GE Healthcare/Amersham Pharmacia Biotech) were used to detect protein signals. Multiple exposures were taken to select images within the dynamic range of the film (GE Healthcare Amersham Hyperfilm ECL). Protein bands were quantified using FIJI software (NIH). Actin or GAPDH bands were used for normalization.

RT-qPCR

RNA was isolated from brain tissue and cell pellets using TRIZol reagent (Thermo Fisher Scientific, Cat# 15596026) and PureLink™ RNA Mini Kit following the manufacturer's instructions. The RNA concentration was determined via Nanodrop and RNA was reverse transcribed using the High-Capacity cDNA Reverse Transcription Kit (Thermo Fisher Scientific, Cat# 4368813). Real time PCR was performed on a Applied Biosystems StepOnePlus Real-Time PCR instrument using 2x TaqMan Universal Master Mix (Cat # 4440040) and gene-specific TaqMan probes against Snca (mouse, Mm01188700_m1), Lrrk2 (mouse, Mm00481934_m1), ActB (Mm02619580_g1), Ifna1 (mouse, Mm03030145_gH), Ifnb1 (mouse, Mm00439552_s1), C3 (mouse, Mm01232779_m1), C1qa (mouse, Mm00432142_m1), Il6 (mouse, Mm00446190_m1), Il1b (mouse, Mm00434228_m1), Tgfb1 (mouse, Mm01178820_m1), Il10 (mouse, Mm01288386_m1), Tnf (mouse, Mm00443258_m1), Trem2 (mouse, Mm04209424_g1), Vim (mouse, Mm01333430_m1), Cxcl10 (mouse, Mm00445235_m1), Cd44 (mouse, Mm01277161_m1), Gfap (mouse, Mm01253033_m1), SNCA (human, Hs01103383_m1), LRRK2 (human, Hs01115057_m1), GRIA1 (human, Hs00181348_m1), MAPT (human, Hs00902194_m1), MAP2 (human, Hs00258900_m1), SNAP25 (human, Hs00938957_m1). ActB was used for normalization. Each sample and primer set was run in triplicates and relative expression level were calculated using the ΔΔCT method.

PFF preparation

The expression and purification of mouse or human wild-type α-syn was performed as previously described. α-Syn fibril formation was induced by incubation in 50mM Tris–HCl, pH 7.5, 150mM KCl buffer at 37°C under continuous shaking in an Eppendorf Thermomixer at 600rpm. α-Syn fibrils were centrifuged twice at 15,000*g* for 10min and resuspended in PBS. For *in vitro* uptake and transport experiments, the fibrils were labeled with Alexa-488 or Alexa-555 (Life Technology, # A-20009) NHS fluorophore following the manufacturer's instructions using a protein:dye ratio of 1:2. The labeling reactions were arrested by addition of 1mM Tris pH 7.5. Free fluorophores were removed by two cycle or centrifugations at 15,000*g* for 10min and resuspension of the pelleted fibrils in PBS. 2.5-5ug of fibrils were used for *in vivo* experiments. 0.01-2ug/ml PFF concentration was used for *in vitro* experiments. All fibrils were fragmented prior to *in vivo* or *in vitro* use by sonication for 20 min in 2-ml Eppendorf tubes in a Vial Tweeter powered by an ultrasonic processor UIS250v (250 W, 2.4 kHz; Hielscher Ultrasonic, Teltow, Germany).

Virus production

HEK293T (ATCC) cells were cultured under standard conditions (DMEM, 10% FBS, penicillin–streptomycin) and used to package lentiviral particles according to standard protocols with third-generation packaging plasmids (pMDlg-pRRE, pRSV-ReV, pMD2.0; Addgene). Lentiviral backbone and packaging plasmids were transfected into HEK293T cells using Lipofectamine 2000 and Lentivirus-containing medium was harvested after 48h. Media was centrifuged at 300*g* for 5min to remove cellular debris, and concentrated using ultracentrifugation (26,000rpm/2hrs/4°C)

or Lenti-X concentrator (Clontech) before being added to cell cultures. ShRNAs were expressed from H1 promoters (pGreenPuro backbone, SystemBio), gRNAs were expressed from U6 promoters. For overexpression experiments, ORFs from the human ORFeome collection were cloned into the pLEX307 destination plasmid (Addgene cat# 41392) using the standard LR clonase protocol (Thermo Fischer Scientific).

Primary Neuron cultures

Primary mouse hippocampal and cortical neurons were dissociated into single-cell suspensions from E16.5 mouse brains with a papain dissociation system (Worthington, Cat# LK003153). Neurons were seeded onto poly-L-lysine–coated plates (0.1% (wt/vol)) and grown in Neurobasal medium (Gibco) supplemented with B-27 serum-free supplement (Gibco), GlutaMAX, and penicillin–streptomycin (Gibco) in a humidified incubator at 37°C, with 5% CO2. Half media changes were performed every 4-5d, or as required. Neurons were plated on 12mm glass coverslips (Carolina Biological Supplies cat# 633009) in 24-well plates (100,000 cells/well), in 12-well plates for biochemical studies (500,000/well), or in 96-well plates for automated imaging and luminescence based survival assays (25,000-35,000 cells/well). For the targeted shRNA-based screens, neurons were grown in clear bottom, black wall plates (Sigma cat# CLS3340-50EA), transduced on 1-3 day in vitro (DIV). For gene-knockout experiments in Cas9 cortical neurons, lentiviruses encoding sgRNAs expressed from a U6 promoter were transduced on 1DIV. Sonicated mouse PFFs were added to neurons on 10DIV. 0.25uM PFFs were used for shRNA-based screens and 0.5uM for internalization experiments. 0.5-1uM PFFs were added to neurons in 24 and 12 well plates, unless otherwise indicated. Neurons were fixed or lysed on 17-21DIV.

ES/iPS and iN culture conditions

ES and iPS cells were cultured using feeder-free conditions on Matrigel (Fisher Scientific cat# CB-40230) using mTeSR1 media (Stemcell Technologies, cat# 85850). ROCK inhibitor Y-27632 was added to the culture media during passaging. Cells were transduced with a Tet-On inducible system allowing for the expression of the transcription factor Ngn2 upon addition of doxycycline to the media. Cells were differentiated as previously described in DMEM/F12 media supplemented with 1x N2 (ThermoFisherScientific) and 1ug/ml doxycycline [63]. Cells were dissociated on day 3-5 of differentiation and replated on poly-L-lysin coated tissue culture plates, glass coverslips or microfluidics chambers (Xona microfluidics SND450). iNs were transitioned to Neurobasal media with 1x B27 and doxycycline starting on day 6. Half media changes were performed every 3-4d, or as required.

Internalization of labelled alpha-synuclein fibrils

The internalization experiments were performed as previously described [9]. Primary mouse neurons or induced neurons were grown in 8 well Lab Tek II chamber slides (ThermoFisherScientific cat# 155409). For induced neurons, sonicated Alexa-488 labeled α-synuclein fibrils were added at a final concentration of 1μM after 14-21 days of differentiation. For primary neurons labeled mouse fibrils were added at a final concentration of 0.5 μM. Internalization was measured at 1, 2, 4, 6, 24 h after the addition of fibrils to the culture media. At each time point, the medium was removed, the cells were washed gently 2-3 times with PBS. 0.1% Trypan blue (ThermoFischerScientific, T10282) was added to each well to quench the non-internalized fluorescent signal and the cells were imaged using a Leica DMI6000B inverted fluorescence microscope with a 20x objective. Control wells without fibrils were used to measure the background fluorescence. 20 images were acquired per well and the percentage of neurons

containing fluorescent puncta as well as the average intensity per neuron was measured using ImageJ. More than 100 neurons were assessed for each well.

Immunocytochemistry

Cells were grown on poly-l-lysine–coated glass coverslips (0.1% (wt/vol) in standard multi-well cell culture plates and were stained through standard immunocytochemistry techniques. Briefly, cells were fixed with 4% formaldehyde for 15 minutes at room temperature, rinsed with PBS, permeabilized with 0.1% Triton X-100, blocked with 5% normal goat serum in PBS. The following primary antibodies were used for labeling: NeuN (1:1000, Millipore cat# MAB377), α-syn pSer129 (1:5000; Covance cat# MMS-5091), α-syn pSer129 (1:3000, Abcam ab51253), α-syn (1:1000, Abcam cat# ab138501), p62 (1:1000; Proteintech cat# 18420-AP), ubiquitin (1:500, Millipore cat# MAB1510), Map2 (1:1000; SYSY cat# 188 004), Map2A/B (1:1000; Millipore cat# MAB378), B-III-tubulin (1:1000; SYSY cat# 303 304). After over-night primary antibody incubation, cells were rinsed 3x with PBS. Cells were incubated with fluorescently labeled secondary antibodies for 1h at room temperature. Coverslips were mounted with Prolong Diamond Antifade mountant with DAPI (Thermo Fisher Scientific). Images were acquired with a Leica DMI6000B inverted fluorescence microscope and a confocal Zeiss LSM710 microscope. Automated imaging and analysis were performed with the IncuCyte life cell analysis imaging system and Molecular Devices ImageXpress Micro and MetaXpress 5. The percentage area of MAP2, BIIItubulin and pSer129 immunofluorescence staining was quantified in ImageJ or MetaXpress 5. The number of NeuN and DAPI labeled-cells were counted using MetaXpress 5 and the analyze particle function in FIJI. The experimentors were blinded to the treatment conditions. For the targeted shRNA based screen, neurons were grown in clear bottom, black wall plates optimized for automated imaging. Images were acquired in a 4x3 grid pattern for each well (12-24 wells/shRNA/screen). The area covered by pSer129 and the number of NeuN-positive nuclei were measured for each image using MetaXpress. Scramble shRNA and untreated control wells were included on each plate. The pSer129 aggregation score was calculated using the pSer129 intensity and area and normalized to the NeuN counts. Scramble controls were included in all plates and used as comparison between plates.

Statistics

Statistical tests were performed with GraphPad Prism 7. Differences between treatment conditions were established using a unpaired Student's t test (for two conditions). For experiments with > 2 groups, a one-way ANOVA with a Tukey's post test for multiple comparisons or two-way ANOVA with Bonferroni correction was performed. Pearson r was calculated for correlation analysis. $p < 0.05$ was considered statistically significant. Statistic details are indicated in the respective figure legends.

Results:

A targeted genetic screen in mouse primary neurons identifies interaction between familial PD genes and α-syn aggregation.

Overexpression of WT α-syn in mouse primary neurons was well tolerated and did not lead to acute degenerative phenotypes (Figure S1a-d). Moreover, transmission of α-syn could be investigated in the absence of overt degeneration using recombinant α-syn PFFs (Figure S1). In this *in vitro* model, the addition of PFFs to neurons induces aggregation of endogenously expressed

α-syn, with synaptic changes and degenerative phenotypes observed only at late stages [40, 57]. We exposed cortical mouse neurons to sonicated α-syn PFFs at 10 days *in vitro* (DIV) and detected aggregation of endogenously expressed α-syn using phospho-Serine129-specific (pSer129) immunolabeling. We first observed pSer129 in neurites after 3 days exposure to PFF. The amount of pSer129 increased progressively over time (Figure S1e,f). We established an automated imaging-based screening approach that combined detection of pSer129 and the neuronal marker NeuN with targeted manipulation of a selection of PD-associated risk genes (Figure S2).

We developed lentiviral shRNA knock down (KD) and overexpression plasmids targeting a variety of PD-linked genes, including Gba1, Lrrk2, Vps35, Synj1, Syt11, Gak, Atp13a2, Pink1, Park2, Park7, Dnajc6, and Dnajc13 (Figure 1a and Figure S2). We infected mouse primary neurons at 1 DIV and measured shRNA-mediated KD at 10 DIV. We included shRNAs that achieved at least 50% KD in further screening. Previously, the level of α-syn expression has been shown to determine the extent of aggregation and mediate selective vulnerability of neuronal populations in PFF-based models of α-syn transmission and aggregation [38, 40, 51, 53, 57]. To assess the dynamic range of the screening assay, we included Snca KD and overexpression conditions as controls. Consistent with previous reports, Snca KD led to a significant reduction in pSer129 levels (Figure 1b,c, Figure S2g), while neuronal overexpression of α-syn led to a two-fold increase (Figure S2g).

For the screen, we infected primary cortical neurons at 1 DIV, added fragmented α-syn PFF at 10 DIV and assessed neuronal pSer129 staining at 20 DIV (Figure 1a). Using pSer129 as a read out, we observed that Gba KD significantly increased α-syn aggregation in primary neurons (Figure 1b,c and Figure S2g). Gba KD also led to an increase in total α-syn levels in the absence of PFF treatment, likely accounting for the observed increase in α-syn aggregation (Figure S3a,b). Interestingly, a feedback loop between Gba and α-syn level has been reported in neurons [42]. Lrrk2 KD led to a significant decrease in pSer129 without changing the total level of α-syn (Figure 1b,c and Figure S2g). We further validated the effect of Lrrk2 KD using Lrrk2-targeting gRNAs in Cas9 transgenic mouse primary neurons. Consistent with our shRNA results, gRNAs targeting endogenous Lrrk2 significantly reduced pSer129 in primary neurons (Figure S3c,d). Importantly, Lrrk2 gRNAs did not alter α-syn levels in the absence of PFF treatment (Figure S3e). Together, these data identify genetic interactions between familial PD genes and α-syn aggregation.

LRRK2 G2019S mutation increases α-syn aggregation in mouse primary neurons.

Mutations in LRRK2, in particular the G2019S mutation, are the most common genetic cause of PD [44, 65]. LRRK2 mutations, including G2019S are thought to cause disease by a gain-of-function mechanism, likely via increased kinase activity [25, 59]. Therefore, we tested whether expression of LRRK2 G2019S would increase α-syn aggregation in the PFF model. We used primary cortical neurons derived from human BAC transgenic mice, expressing LRRK2 under the control of the endogenous human regulatory elements [58]. Using the PFF-based aggregation assay, we observed a significant increase in pSer129 levels in neurons from LRRK2 G2019S transgenic mice compared to WT controls (Figure 1e). Importantly, LRRK2 G2019S did not alter expression of endogenous α-syn or other synaptic proteins in primary neurons (Figure 1f and S3g,h). Additionally, we did not observe any differences in cellular toxicity between LRRK2 G2019S mutant and WT PFF-treated neurons (Figure S3i,j). Considering that several Rab GTPases have recently been identified as LRRK2 kinase substrates, potentially modulating α-syn uptake, trafficking, escape from the endo-lysosomal compartment and aggregation, we next measured the internalization kinetics of α-syn fibrils [3, 5, 19, 52]. However, we did not observe any significant differences in uptake or endocytosis of α-syn PFFs between LRRK2 G2019S mutant and WT neurons (Figure S3k). These data indicate that expression of LRRK2 G2019S is associated with

increased α-syn aggregation without impacting internalization of PFF or expression of endogenous α-syn in mouse primary neurons.

PFF injection into the striatum induces α-syn aggregation and degeneration in mice.
Previous reports have demonstrated that local PFF delivery into the striatum of rodents induces aggregation of endogenously expressed α-syn in remote brain areas projecting to the injection site, including the SNpc [38, 46]. PFF-based *in vivo* mouse models allow for both the ability to perform longitudinal studies, as well as to assess diverse neuronal populations and the complex interplay between neurons and glial cells in the context of neurodegeneration [40, 60]. We harnessed this model to test the impact of LRRK2 G2019S on α-syn aggregation and degeneration. We first used unilateral stereotaxic injections to deliver fragmented mouse PFFs or vehicle control into the striatum of non-transgenic adult mice, followed by behavioral testing and histological analysis up to 6 months post injection (Figure S4a). Consistent with previous reports [38], PFF-injected mice developed widespread pSer129-positive and p62-positive inclusions in both hemispheres (Figure S4b) in regions that include the cortex, amygdala, and striatum. Importantly, TH-positive dopaminergic neurons in the SNpc, an area associated with movement dysfunction in human PD, developed robust α-syn pathology ipsilateral to the injection site (Figure S4c). Further, we observed a significant decrease in the number of TH-positive neurons in the SNpc 4-6 months post injection (Figure S4d-f). In contrast to previous reports [37, 38, 41, 46, 60], we did not observe robust deficits in behavioral paradigms testing motor control and coordination (Figure S4g). However, mice injected with PFFs displayed altered anxiety-related behavior in the open field test at 6 months post injection. While there was no difference in overall activity and distance travelled, mice injected with PFFs spent significantly more time in the center as opposed to vehicle injected mice (Figure S4h). Cumulatively, the PFF-based mouse model mimicked key histopathological features of PD.

LRRK2 G2019S expression exacerbates PFF-mediated α-syn aggregation and degeneration pathology in mice.
Having established the PFF-based *in vivo* model, we next investigated the role of human LRRK2 G2019S in aggregation of α-syn in the basal ganglia circuitry, degeneration of TH neurons and behavior. We used human LRRK2 BAC-transgenic mice, expressing the G2019S mutant form of LRRK2 using human regulatory elements (Figure 2a,b). LRRK2 G2019S transgenic mice developed normally and no significant differences in α-syn expression, motor function and body weight were detected in up to 12-month-old transgenic animals compared to WT littermate (Figure S5). For subsequent experiments, LRRK2 G2019S transgenic mice and WT littermates were stereotaxically injected bilaterally into the striatum with α-syn PFFs or vehicle control, followed by behavioral testing and histological analysis at 1, 3 and 6 months post-injection (Figure 2a,b).

At 1 month post-injection, the LRRK2 G2019S transgenic mice displayed significantly more pSer129 aggregates in the dorsal striatum, motor cortex and amygdala. However, by 3 and 6 months post-injection, both LRRK2 G2019S transgenic animals and WT controls developed widespread pSer129-positive inclusions in the brain. No pSer129-positive inclusions were detected in either vehicle injected LRRK2 G2019S transgenic or WT control animals at any time point. In the SNpc, the percentage of TH-positive pSer129-positive neurons was significantly higher in LRRK2 G2019S transgenic mice at 1 month post injection compared to WT controls (Figure 2c,d). Although a significant difference in pSer129 expression persisted up to 6 months post-injection, the relative differences between the two groups decreased over time (Figure 2c,d). As previously observed in WT animals (Figure S4c), the percentage of TH-positive dopaminergic neurons co-labeled with pSer129 decreased between 3 and 6 months post-injection for both

genotypes (Figure 2d). Using stereological analysis of TH-positive neuronal cell bodies in the SNpc, we observed accelerated loss of TH-positive neurons in LRRK2 G2019S transgenic mice compared to WT littermate controls at 3 months post-injection that was further exacerbated at 6 months post-injection (Figure 2e). Importantly, we did not observe any degeneration of TH-neurons in vehicle injected animals. Together, these findings indicate an accelerated degenerative phenotype in LRRK2 G2019S transgenic mice, with increased α-syn pathology and loss of TH-positive neurons occurring in the SNpc at early time points.

Protein aggregation and neuronal cell loss is often associated with neuroinflammation in human neurodegenerative diseases and mouse models of neurodegeneration. Moreover, a recent study demonstrated a role for microglia and astrocytes in the development of α-syn pathology in mouse models of PD [60]. Given ubiquitous expression of LRRK2 in the human and mouse CNS, including in neurons and glial cells [62], we next examined changes in glial activation in LRRK2 G2019S transgenic and WT animals following PFF injection. While we detected increased microglia activation in both PFF-injected LRRK2 G2019S transgenic and WT control mice, as assessed by Iba1 expression, we observed altered microglia morphology selectively in LRRK2 G2019S transgenic mice (Figure S6a-d). Additionally, using RT-qPCR analysis, we observed increased levels of inflammatory markers Il6, Tnfa and C1qa, as well as astrocytic markers Vim, Cd44 and Cxcl10 in LRRK2 G2019S transgenic animals compared to WT controls (Figure S6e-g). Histologically, we also observed elevated C1q expression in PFF injected LRRK2 G2019S transgenic mice compared to WT controls (Figure S6h,i). Together, these data identify accompanying neuroinflammatory phenotypes in PFF-injected LRRK2 G2019S transgenic mice.

Lastly, we investigated whether increased α-syn aggregation and dopaminergic neuron degeneration observed in PFF-injected LRRK2 G2019S transgenic mice was associated with behavioral deficits at 6 months post injection. Using the open field test, we observed that PFF-injected LRRK2 G2019S transgenic mice spent more time in the center than WT control animals (Figure 2f). Additionally, using rotarod testing, we assessed motor behavior and coordination. We observed a significant decrease in the ability of LRRK2 G2019S transgenic mice to stay on a rotating cylinder compared to WT controls (Figure 2g). Collectively, these behavioral data indicate decreased anxiety phenotypes and increased motor impairments in α-syn PFF-injected LRRK2 G2019S transgenic mice.

Establishing a model of α-syn aggregation and transmission in human induced neurons

In addition to rodents, fibril based aggregation models have been reported in marmosets and rhesus macaques, demonstrating that transmission in primate models is possible [39, 45, 48, 50]. To evaluate the role of LRRK2 in α-syn transmission in the context of human pathology, we developed an *in vitro* model of PFF-induced α-syn aggregation in human neurons. A key limitation in PFF-based models is the dependency on expression of endogenous α-syn [38, 40, 53]. Moreover, due to its predominant pre-synaptic localization α-syn expression is further dependent on neuronal maturation and synaptogenesis. Differentiation and maturation of human ES/iPS-derived neurons is often a relatively inefficient, laborious and lengthy process, yielding heterogenous populations of neurons that are not ideal for PFF-based *in vitro* models. To circumvent technical limitations and avoid the confounds linked to α-syn overexpression, we employed an induced neuron (iN) approach previously shown to rapidly differentiate human ES/iPS cells into functional cortical neurons (Figure S7a) [63]. Human iPS cells differentiated rapidly into iNs with neuronal morphology, expressing neuronal markers NeuN, BIII-tubulin, TAU and MAP2 (Figure S7b,c). Additionally, α-syn expression significantly increased over the first 2 weeks of differentiation (Figure S7d,e), in line with neurite and synaptic markers (Figure S7f-i).

Previous reports indicate a species-dependent barrier between mouse and human fibrils, potentially impacting cross-seeding and templating efficiency [37]. Therefore, we treated human neurons with fragmented human α-syn PFFs. Consistent with our mouse primary neuron experiments, we added human PFFs to 2-3 week-old iNs and performed pSer129 immunolabeling at various time points following fibril treatment (Figure 3a). Starting at approximately 6-10 days post fibril treatment, we detected elongated and serpentine-like pSer129 staining in PFF - but not vehicle-treated iNs. Levels of pSer129 labeling significantly increased with time (Figure 3b,c), resembling α-syn inclusions observed at early stages in mouse primary neurons treated with mouse fibrils, although the pathology developed with slower kinetics in human iNs (Figure S1e,f). Elongated pSer129-positive structures resembled Lewy neurites and predominantly co-localized with the axonal markers BIII-tubulin and Tau (Figure 3d). Phosphorylated aggregates also partially co-localized with ubiquitin, similar to observations in mouse primary neurons (Figure 3e) [57]. Additionally, we sequentially extracted and immunoblotted lysates from human iNs exposed for 14 days with human PFFs in 1% Triton X followed by 2% SDS, and detected pSer129 predominantly in the SDS resistant fraction. Collectively, these data indicate that PFFs trigger aggregation of endogenous α-syn in human iNs.

LRRK2 G2019S mutation and LRRK2 expression modulate α-syn transmission and aggregation in fPD patient-derived human induced neurons.

We next used our human neuron-based PFF model to investigate uptake and aggregation of α-syn in LRRK2 mutant iNs. We used fPD patient-derived human iPS cells from LRRK2 G2019S carriers, isogenic gene corrected lines and isogenic LRRK2 KO lines [49]. We first confirmed expression of LRRK2 and the presence of the G2019S mutation in all isogenic lines (Figure S8a). We differentiated all lines and did not observe any difference in survival between G2019S mutant, corrected and LRRK2 KO human iNs (Figure S8b,c). We then measured the internalization of α-syn PFFs by human iNs (Figure 4a-c). After 24 hours, approximately 95% of human iNs contained fluorescently labeled α-syn PFFs. We did not observe any significant difference between LRRK2 mutant and isogenic corrected lines, indicating that LRRK2 expression and activity did not significantly alter α-syn PFF internalization in human iNs (Figure 4c).

We next used the PFF transmission model to investigate aggregation of endogenously expressed α-syn. We compared pSer129 labeling between G2019S mutant, corrected and LRRK2 KO human iNs. We observed a significant increase in pSer129 in G2019S mutant human iNs, consistent with our findings in mouse primary neurons (Figure 1d-f). Surprisingly, LRRK2 KO human neurons displayed a significant reduction in pSer129 (Figure 4d,e). We corroborated these findings in lysates from human iNs two weeks post exposure to fibril, detecting increased pSer129 in G2019S mutant compared to corrected human iNs in the 2% SDS fraction. Conversely, pSer129 was decreased in lysates from LRRK2 KO human iNs (Figure 4f,g). We did not observe any significant differences in the pre- and postsynaptic markers Synaptophysin and PSD95 in PFF treated human iNs (Figure 4h,i). Given the extent of α-syn aggregation is sensitive to endogenous expression level, we measured and detected comparable α-syn levels between G2019S mutant and corrected human iNs independent of PFF treatment (Figure 5a,b). Surprisingly, the amount of α-syn was decreased in LRRK2 KO compared to G2019S mutant and corrected human neurons, potentially accounting for decreased pSer129 levels observed in LRRK2 KO iNs. Due to the synaptic localization of endogenous α-syn, we next examined whether there were differences in neuronal maturation and synaptogenesis between G2019S mutant, corrected and LRRK2 KO human iNs. Interestingly, we did not observe any differences in the levels of other synaptic markers, including Synaptophysin, Homer1 and PSD95 (Figure 5b-e). Furthermore, the differentiation-dependent upregulation of neuronal and synaptic markers was comparable between

the different human isogenic lines, as assessed using previously identified pan-neuronal and mature neuron markers (Figure 5f-i) [54]. Together, these data demonstrate that PFFs can seed aggregation of endogenously expressed α-syn in fPD-derived human iNs. Importantly, both the G2019S mutation, as well as LRRK2 expression level, modulated α-syn aggregation in this human *in vitro* model of PFF-based transmission, indicating a conserved role for genetic interaction between fPD genes and α-syn aggregation across mouse and human models.

Discussion:

In our study, we employed a targeted screen of PD-associated risk genes to identify LRRK2 as a mediator of α-syn transmission and aggregation. We demonstrated that abrogation of endogenous Lrrk2 in mouse primary neurons decreases α-syn aggregates, whereas expression of the familial PD-associated G2019S mutation increases aggregation. *In vivo*, transgenic mouse data demonstrated that expression of LRRK2 G2019S exacerbates α-syn aggregation, dopaminergic neuron degeneration, as well as associated neuroinflammatory and behavioral impairments in a PFF-based mouse model of PD. We extended these observations by developing and characterizing an *in vitro* human neuron PFF-based transmission model. Using human iPS-derived induced neurons, we observed that human neurons rapidly internalize recombinant human PFFs, triggering the aggregation of endogenously expressed α-syn. We demonstrate that the LRRK2 G2019S mutation increases formation of α-syn aggregates in human iNs derived from fPD patients. Conversely, loss of LRRK2 decreased α-syn aggregation in human iNs. Ultimately, our data posit reduction of LRRK2 as a potential therapeutic approach to mitigate α-syn aggregation and promote neuronal integrity. Clinical trials of LRRK2 kinase inhibitors are currently underway [3, 21]. Interestingly, increased LRRK2 kinase activity has recently been reported in sporadic PD [16]. Our results showing that LRRK2 knockout decreases aggregation of α-syn raises the possibility that these inhibitors may be efficacious in sporadic PD and not only in PD cases caused by LRRK2 mutations.

Our PD risk gene-specific imaging-based screen described in our study enabled us to assess α-syn aggregation independent of toxicity and survival of primary neurons. Though focused in scope, our targeted screen successfully identified Gba and Lrrk2 as potential modifiers of PFF transmission and aggregation of α-syn. Interestingly, genes associated with juvenile forms of PD, such as Pink1 and Park2, which are not robustly associated with Lewy body pathology, exhibited no effects in this assay. Given the specificity of this imaging-based screen, its application could be expanded to identify additional modifiers or small molecule inhibitors of α-syn transmission and aggregation.

There are strong experimental and epidemiological evidence linking α-syn aggregation directly to endogenous levels of α-syn expression [38, 40]. In particular, genetic duplications and triplications of the *SNCA* locus are a genetic cause of fPD with exacerbated α-syn aggregation pathology and earlier disease onset [11, 51]. Through our screen, we demonstrated that knock down of Gba increased α-syn level in mouse primary neurons, possibly accounting for the observed increase in α-syn aggregation in response to PFF treatment. Consistent with our findings, interactions between Gba and α-syn levels have previously been reported in cell lines and primary neurons [2, 27, 42]. Moreover, GBA mutations are one of the most common genetic risk factors for PD in humans [65].

A growing number of animal models have been developed to further our understanding of pathogenesis of PD-associated LRRK2 mutations and α-syn aggregation. However, strong

neuronal overexpression of both LRRK2 and human α-syn have yielded conflicting reports [13, 14, 30, 36]. It is unclear to what extent neuronal overexpression reflects the human pathology, given the ubiquitous expression of LRRK2 in the CNS in both neuronal and glial cells [62]. Additionally, PD is not commonly associated with elevated expression of α-syn, and overexpression of human α-syn can lead to toxic effects in eukaryotic cells independent of the formation of α-syn aggregates [12]. Recently, two studies investigated the effect of LRRK2 mutations using PFF-based *in vitro* models, with both observing an increase in α-syn aggregation in primary neurons using the same transgenic mouse LRRK2 BAC line [28, 55]. Surprisingly, they report conflicting observations regarding the level of endogenously expressed α-syn protein level and the efficiency of LRRK2 inhibition in their mutant LRRK2 neurons. Although we initially identified the interaction between Lrrk2 and α-syn transmission in our targeted screen independent of the G2019S mutation, using a complementary human LRRK2 G2019S BAC-transgenic mouse strain we observe an increase in α-syn aggregation in primary neurons, in agreement with Volpicelli *et al.* and Henderson *et al* [28, 55]. We further extended our studies *in vivo*, delivering PFFs into the dorsal striatum of adult LRRK2 G2019S transgenic mice and observed accelerated α-syn aggregation and degeneration of TH neurons in our 6 month longitudinal study. Additionally, we observed an increase in the number of dopaminergic neurons with α-syn inclusions. Our findings are bolstered by a recent study in which PFFs were directly injected into the SNpc of rats, although this study does not account for transmission and transport of α-syn from a remote injection site to the site of aggregation [55]. Interestingly, while the distribution and extent of α-syn pathology was surprisingly similar between LRRK2 and WT mice at 6 months post injection, we observed differing neuroinflammatory and glial responses in LRRK2 mutant mice at the same time point. Based on the growing knowledge of neuron-glia interaction in homeostasis, aging and neurodegenerative diseases, it is possible that glial cells could, in part, contribute to the accelerated phenotypes and impaired behavior observed in LRRK2 G2019S transgenic mice. Indeed, glial cells have recently been shown to contribute to α-syn pathology in a PFF-based mouse model [60], and several studies have proposed potential immune-related roles for LRRK2. For example, altered inflammatory and degenerative phenotypes have been reported in LRRK2-mutant rodents following LPS challenges [15, 43]. Taken together, these findings warrant further investigations into the relationship between LRRK2 mutations, accelerated α-syn pathology, and glial cells in models of PD.

Because of the success of PFF-based *in vitro* and *in vivo* mouse models and the increasing availability of human PD-iPS lines, we set out to develop a PFF-based *in vitro* model for human neurons. We used a rapid induced neuron paradigm, allowing for the rapid differentiation of iPS cells into iNs, which developed α-syn aggregates in response to PFF treatment. As primarily a synaptic protein, α-syn is upregulated with increased maturation and synaptogenesis during differentiation. Importantly, we observed a significant increase in α-syn level and aggregation within a few weeks of differentiation without the need for α-syn overexpression. An intriguing distinction pertaining to PD between humans and rodents is the difference in the amino acid sequence of α-syn. The A53T mutation, associated with familial PD in humans, is the native amino acid sequence in mice and rats, possibly accounting for accelerated aggregation in rodent neurons [47]. Further, familial PD is associated with an earlier onset and more severe aggregation phenotype in subjects with the A53T mutation [22]. Given disparities between mouse and human models of PD at a fundamental structural level with respect to α-syn, it is critical to translate findings in animal models to a human disease context. To that end, various iPS and fibroblast-based protocols have recently been developed, potentially allowing for the generation of different neuronal subtypes that include those associated with individual degenerative diseases [26, 54]. Furthermore, the relative ease of use, the homogeneity of the neuron cultures and the ability to

generate sufficiently high numbers of cells make iNs strong candidates for novel human neuron-based platforms to interrogate underlying mechanisms of disease progression and identification of potential therapeutic targets. Indeed, we demonstrated that loss of LRRK2 decreased α-syn aggregation in PFF-treated fPD patient-derived iNs, complementing results from *in vivo* antisense oligonucleotide (ASO) approaches in mice [64], and lending credence to the suitability of LRRK2 as a potential drug target.

Acknowledgements
This work was supported by the National Institutes of Health grant R35NS097263 (A.D.G), Stanford BioX (A.D.G), research funding from Novartis Institutes of Biomedical Research (A.D.G), Stanford Graduate Fellowship (GB), HHMI fellowship (GB). RM and LB lab was supported by Grants from the EC Joint Programme on Neurodegenerative Diseases (JPND-SYNACTION-ANR-15-JPWG-0012-03), the Fondation pour la Recherche Médicale (Contract DEQ 20160334896) and the Innovative Medicine Initiative 2 grant agreement No 116060 (IMPRiND, www.imprind.org) supported by the European Union's Horizon 2020 research and innovation program and EFPIA. The generation of the patient-specific ZFN-modified LRRK2 lines were supported by the California Institute of Regenerative Medicine (RT2-0196, BS). We thank Dr. Marius Wernig and Dr Daniel Haag for providing the TetOn and Ngn2 plasmids and advice with the induced neuron platform, Dr. Herschel and Dr. Suzanne Pfeffer for advice on LRRK2 expression and activity assays and Dr. Laura Volpicelli-Daley for advice on pSer129 immunostainings and immunoblotting. We thank A. Olsen and the Stanford Neuroscience Microscopy Service, supported by a grant from NIH (NS069375) and J. Mulholland from the CSIF for help with microscopy and image acquisition, Y. Zuber (Stanford Veterinary Service Center) for mouse husbandry advice and support, the High Throughput Bio-Science center for providing access to imaging and analysis tools.

Conflict of interest
The authors declare that they have no conflict of interest.

Ethical approval
All applicable international, national, and/or institutional guidelines for the care and use of animals were followed. All procedures involving animals were in accordance with the ethical standards set by the Administrative Panel on Laboratory Animal Care of Stanford University (APLAC). This article does not contain any study with human participants performed by any of the authors.

References:

1. Abeliovich A, Gitler AD (2016) Defects in trafficking bridge Parkinson's disease pathology and genetics. Nature 539:207–216. doi: 10.1038/nature20414

2. Aflaki E, Westbroek W, Sidransky E (2017) The Complicated Relationship between Gaucher Disease and Parkinsonism: Insights from a Rare Disease. NEURON 93:737–746. doi: 10.1016/j.neuron.2017.01.018

3. Alessi DR, Sammler E (2018) LRRK2 kinase in Parkinson's disease. Science 360:36–37. doi: 10.1126/science.aar5683

4. Appel-Cresswell S, Vilarino-Guell C, Encarnacion M, Sherman H, Yu I, Shah B, Weir D, Thompson C, Szu-Tu C, Trinh J, Aasly JO, Rajput A, Rajput AH, Jon Stoessl A, Farrer MJ (2013) Alpha-synuclein p.H50Q, a novel pathogenic mutation for Parkinson's disease. Mov Disord 28:811–813. doi: 10.1002/mds.25421

5. Bae E-J, Kim D-K, Kim C, Mante M, Adame A, Rockenstein E, Ulusoy A, Klinkenberg M, Jeong GR, Bae JR, Lee C, Lee H-J, Lee B-D, Di Monte DA, Masliah E, Lee S-J (2018) LRRK2 kinase regulates α-synuclein propagation via RAB35 phosphorylation. Nat Commun 9:3465. doi: 10.1038/s41467-018-05958-z

6. Bieri G, Gitler AD, Brahic M (2018) Internalization, axonal transport and release of fibrillar forms of alpha-synuclein. Neurobiol Dis 109:219–225. doi: 10.1016/j.nbd.2017.03.007

7. Braak H, Del Tredici K, Bratzke H, Hamm-Clement J, Sandmann-Keil D, Rüb U (2002) Staging of the intracerebral inclusion body pathology associated with idiopathic Parkinson's disease (preclinical and clinical stages). J Neurol 249:iii1–iii5. doi: 10.1007/s00415-002-1301-4

8. Braak H, Del Tredici K, Rüb U, de Vos RAI, Jansen Steur ENH, Braak E (2003) Staging of brain pathology related to sporadic Parkinson's disease. Neurobiol Aging 24:197–211.

9. Brahic M, Bousset L, Bieri G, Melki R, Gitler AD (2016) Axonal transport and secretion of fibrillar forms of α-synuclein, Aβ42 peptide and HTTExon 1. Acta Neuropathol 1–10. doi: 10.1007/s00401-016-1538-0

10. Chang D, Nalls MA, Hallgrímsdóttir IB, Hunkapiller J, van der Brug M, Cai F, International Parkinson's Disease Genomics Consortium, 23andMe Research Team, Kerchner GA, Ayalon G, Bingol B, Sheng M, Hinds D, Behrens TW, Singleton AB, Bhangale TR, Graham RR (2017) A meta-analysis of genome-wide association studies identifies 17 new Parkinson's disease risk loci. Nature Genetics 49:1511–1516. doi: 10.1038/ng.3955

11. Chartier-Harlin M-C, Kachergus J, Roumier C, Mouroux V, Douay X, Lincoln S, Levecque C, Larvor L, Andrieux J, Hulihan M, Waucquier N, Defebvre L, Amouyel P,

Farrer M, Destée A (2004) Alpha-synuclein locus duplication as a cause of familial Parkinson's disease. Lancet 364:1167–1169. doi: 10.1016/S0140-6736(04)17103-1

12. Cooper AA, Gitler AD, Cashikar A, Haynes CM, Hill KJ, Bhullar B, Liu K, Xu K, Strathearn KE, Liu F, Cao S, Caldwell KA, Caldwell GA, Marsischky G, Kolodner RD, Labaer J, Rochet J-C, Bonini NM, Lindquist S (2006) Alpha-synuclein blocks ER-Golgi traffic and Rab1 rescues neuron loss in Parkinson's models. Science 313:324–328. doi: 10.1126/science.1129462

13. Daher JPL, Abdelmotilib HA, Hu X, Volpicelli-Daley LA, Moehle MS, Fraser KB, Needle E, Chen Y, Steyn SJ, Galatsis P, Hirst WD, West AB (2015) Leucine-rich Repeat Kinase 2 (LRRK2) Pharmacological Inhibition Abates α-Synuclein Gene-induced Neurodegeneration. Journal of Biological Chemistry 290:19433–19444. doi: 10.1074/jbc.M115.660001

14. Daher JPL, Pletnikova O, Biskup S, Musso A, Gellhaar S, Galter D, Troncoso JC, Lee MK, Dawson TM, Dawson VL, Moore DJ (2012) Neurodegenerative phenotypes in an A53T α-synuclein transgenic mouse model are independent of LRRK2. Hum Mol Genet 21:2420–2431. doi: 10.1093/hmg/dds057

15. Daher JPL, Volpicelli-Daley LA, Blackburn JP, Moehle MS, West AB (2014) Abrogation of α-synuclein-mediated dopaminergic neurodegeneration in LRRK2-deficient rats. Proc Natl Acad Sci USA 111:9289–9294. doi: 10.1073/pnas.1403215111

16. Di Maio R, Hoffman EK, Rocha EM, Keeney MT, Sanders LH, De Miranda BR, Zharikov A, Van Laar A, Stepan AF, Lanz TA, Kofler JK, Burton EA, Alessi DR, Hastings TG, Greenamyre JT (2018) LRRK2 activation in idiopathic Parkinson's disease. Science Translational Medicine 10:eaar5429. doi: 10.1126/scitranslmed.aar5429

17. Dickson DW (2012) Parkinson's disease and parkinsonism: neuropathology. Cold Spring Harb Perspect Med 2:a009258–a009258. doi: 10.1101/cshperspect.a009258

18. Flagmeier P, Meisl G, Vendruscolo M, Knowles TPJ, Dobson CM, Buell AK, Galvagnion C (2016) Mutations associated with familial Parkinson's disease alter the initiation and amplification steps of α-synuclein aggregation. Proc Natl Acad Sci USA 113:10328–10333. doi: 10.1073/pnas.1604645113

19. Flavin WP, Bousset L, Green ZC, Chu Y, Skarpathiotis S, Chaney MJ, Kordower JH, Melki R, Campbell EM (2017) Endocytic vesicle rupture is a conserved mechanism of cellular invasion by amyloid proteins. Acta Neuropathol 35:2120–25. doi: 10.1007/s00401-017-1722-x

20. Freundt EC, Maynard N, Clancy EK, Roy S, Bousset L, Sourigues Y, Covert M, Melki R, Kirkegaard K, Brahic M (2012) Neuron-to-neuron transmission of α-synuclein fibrils through axonal transport. Ann Neurol 72:517–524. doi: 10.1002/ana.23747

21. Fuji RN, Flagella M, Baca M, Baptista MAS, Brodbeck J, Chan BK, Fiske BK, Honigberg L, Jubb AM, Katavolos P, Lee DW, Lewin-Koh S-C, Lin T, Liu X, Liu S, Lyssikatos JP, O'Mahony J, Reichelt M, Roose-Girma M, Sheng Z, Sherer T, Smith A, Solon M,

Sweeney ZK, Tarrant J, Urkowitz A, Warming S, Yaylaoglu M, Zhang S, Zhu H, Estrada AA, Watts RJ (2015) Effect of selective LRRK2 kinase inhibition on nonhuman primate lung. Science Translational Medicine 7:273ra15–273ra15. doi: 10.1126/scitranslmed.aaa3634

22. Fujioka S, Ogaki K, Tacik PM, Uitti RJ, Ross OA, Wszolek ZK (2014) Update on novel familial forms of Parkinson's disease and multiple system atrophy. Parkinsonism Relat Disord 20 Suppl 1:S29–34. doi: 10.1016/S1353-8020(13)70010-5

23. Goedert M, Spillantini MG, Del Tredici K, Braak H (2013) 100 years of Lewy pathology. Nat Rev Neurol 9:13–24. doi: 10.1038/nrneurol.2012.242

24. Goetz CG (2011) The History of Parkinson's Disease: Early Clinical Descriptions and Neurological Therapies. Cold Spring Harb Perspect Med 1:a008862–a008862. doi: 10.1101/cshperspect.a008862

25. Greggio E, Jain S, Kingsbury A, Bandopadhyay R, Lewis P, Kaganovich A, van der Brug MP, Beilina A, Blackinton J, Thomas KJ, Ahmad R, Miller DW, Kesavapany S, Singleton A, Lees A, Harvey RJ, Harvey K, Cookson MR (2006) Kinase activity is required for the toxic effects of mutant LRRK2/dardarin. Neurobiol Dis 23:329–341. doi: 10.1016/j.nbd.2006.04.001

26. Gribaudo S, Tixador P, Bousset L, Fenyi A, Lino P, Melki R, Peyrin J-M, Perrier AL (2019) Propagation of α-Synuclein Strains within Human Reconstructed Neuronal Network. Stem Cell Reports. doi: 10.1016/j.stemcr.2018.12.007

27. Gündner AL, Duran-Pacheco G, Zimmermann S, Ruf I, Moors T, Baumann K, Jagasia R, van de Berg WDJ, Kremer T (2018) Path mediation analysis reveals GBA impacts Lewy body disease status by increasing α-synuclein levels. Neurobiol Dis. doi: 10.1016/j.nbd.2018.09.015

28. Henderson MX, Peng C, Trojanowski JQ, Lee VMY (2018) LRRK2 activity does not dramatically alter α-synuclein pathology in primary neurons. Acta Neuropathol Commun 6:45. doi: 10.1186/s40478-018-0550-0

29. Hernandez DG, Reed X, Singleton AB (2016) Genetics in Parkinson disease: Mendelian versus non-Mendelian inheritance. J Neurochem 139 Suppl 1:59–74. doi: 10.1111/jnc.13593

30. Herzig MC, Bidinosti M, Schweizer T, Hafner T, Stemmelen C, Weiss A, Danner S, Vidotto N, Stauffer D, Barske C, Mayer F, Schmid P, Rovelli G, van der Putten PH, Shimshek DR (2012) High LRRK2 levels fail to induce or exacerbate neuronal alpha-synucleinopathy in mouse brain. PLoS ONE 7:e36581. doi: 10.1371/journal.pone.0036581

31. Jucker M, Walker LC (2013) Self-propagation of pathogenic protein aggregates in neurodegenerative diseases. Nature 501:45–51. doi: 10.1038/nature12481

32. Kalia LV, Lang AE (2015) Parkinson's disease. Lancet 386:896–912. doi: 10.1016/S0140-6736(14)61393-3

33. Kiely AP, Asi YT, Kara E, Limousin P, Ling H, Lewis P, Proukakis C, Quinn N, Lees AJ, Hardy J, Revesz T, Houlden H, Holton JL (2013) α-Synucleinopathy associated with G51D SNCA mutation: a link between Parkinson's disease and multiple system atrophy? Acta Neuropathol 125:753–769. doi: 10.1007/s00401-013-1096-7

34. Krüger R, Kuhn W, Müller T, Woitalla D, Graeber M, Kösel S, Przuntek H, Epplen JT, Schöls L, Riess O (1998) Ala30Pro mutation in the gene encoding alpha-synuclein in Parkinson's disease. Nature Genetics 18:106–108. doi: 10.1038/ng0298-106

35. Lee BR, Kamitani T (2011) Improved immunodetection of endogenous α-synuclein. PLoS ONE 6:e23939. doi: 10.1371/journal.pone.0023939

36. Lin X, Parisiadou L, Gu X-L, Wang L, Shim H, Sun L, Xie C, Long C-X, Yang W-J, Ding J, Chen ZZ, Gallant PE, Tao-Cheng J-H, Rudow G, Troncoso JC, Liu Z, Li Z, Cai H (2009) Leucine-rich repeat kinase 2 regulates the progression of neuropathology induced by Parkinson's-disease-related mutant alpha-synuclein. NEURON 64:807–827. doi: 10.1016/j.neuron.2009.11.006

37. Luk KC, Covell DJ, Kehm VM, Zhang B, Song IY, Byrne MD, Pitkin RM, Decker SC, Trojanowski JQ, Lee VMY (2016) Molecular and Biological Compatibility with Host Alpha-Synuclein Influences Fibril Pathogenicity. Cell Rep 16:3373–3387. doi: 10.1016/j.celrep.2016.08.053

38. Luk KC, Kehm V, Carroll J, Zhang B, O'Brien P, Trojanowski JQ, Lee VMY (2012) Pathological α-synuclein transmission initiates Parkinson-like neurodegeneration in nontransgenic mice. Science 338:949–953. doi: 10.1126/science.1227157

39. Luk KC, Kehm VM, Zhang B, O'Brien P, Trojanowski JQ, Lee VMY (2012) Intracerebral inoculation of pathological α-synuclein initiates a rapidly progressive neurodegenerative α-synucleinopathy in mice. J Exp Med 209:975–986. doi: 10.1084/jem.20112457

40. Luna E, Decker SC, Riddle DM, Caputo A, Zhang B, Cole T, Caswell C, Xie SX, Lee VMY, Luk KC (2018) Differential α-synuclein expression contributes to selective vulnerability of hippocampal neuron subpopulations to fibril-induced toxicity. Acta Neuropathol 105:84–21. doi: 10.1007/s00401-018-1829-8

41. Mao X, Ou MT, Karuppagounder SS, Kam T-I, Yin X, Xiong Y, Ge P, Umanah GE, Brahmachari S, Shin J-H, Kang HC, Zhang J, Xu J, Chen R, Park H, Andrabi SA, Kang SU, Gonçalves RA, Liang Y, Zhang S, Qi C, Lam S, Keiler JA, Tyson J, Kim D, Panicker N, Yun SP, Workman CJ, Vignali DAA, Dawson VL, Ko HS, Dawson TM (2016) Pathological α-synuclein transmission initiated by binding lymphocyte-activation gene 3. Science 353:aah3374–aah3374. doi: 10.1126/science.aah3374

42. Mazzulli JR, Xu Y-H, Sun Y, Knight AL, McLean PJ, Caldwell GA, Sidransky E, Grabowski GA, Krainc D (2011) Gaucher disease glucocerebrosidase and α-synuclein

form a bidirectional pathogenic loop in synucleinopathies. Cell 146:37–52. doi: 10.1016/j.cell.2011.06.001

43. Moehle MS, Daher JPL, Hull TD, Boddu R, Abdelmotilib HA, Mobley J, Kannarkat GT, Tansey MG, West AB (2015) The G2019S LRRK2 mutation increases myeloid cell chemotactic responses and enhances LRRK2 binding to actin-regulatory proteins. Hum Mol Genet 24:4250–4267. doi: 10.1093/hmg/ddv157

44. Paisán-Ruíz C, Jain S, Evans EW, Gilks WP, Simón J, van der Brug M, López de Munain A, Aparicio S, Gil AM, Khan N, Johnson J, Martinez JR, Nicholl D, Carrera IM, Pena AS, de Silva R, Lees A, Martí-Massó JF, Pérez-Tur J, Wood NW, Singleton AB (2004) Cloning of the gene containing mutations that cause PARK8-linked Parkinson's disease. NEURON 44:595–600. doi: 10.1016/j.neuron.2004.10.023

45. Paumier KL, Luk KC, Manfredsson FP, Kanaan NM, Lipton JW, Collier TJ, Steece-Collier K, Kemp CJ, Celano S, Schulz E, Sandoval IM, Fleming S, Dirr E, Polinski NK, Trojanowski JQ, Lee VM, Sortwell CE (2015) Intrastriatal injection of pre-formed mouse α-synuclein fibrils into rats triggers α-synuclein pathology and bilateral nigrostriatal degeneration. Neurobiol Dis 82:185–199. doi: 10.1016/j.nbd.2015.06.003

46. Peelaerts W, Bousset L, Van der Perren A, Moskalyuk A, Pulizzi R, Giugliano M, Van den Haute C, Melki R, Baekelandt V (2015) α-Synuclein strains cause distinct synucleinopathies after local and systemic administration. Nature 522:340–344. doi: 10.1038/nature14547

47. Polymeropoulos MH, Lavedan C, Leroy E, Ide SE, Dehejia A, Dutra A, Pike B, Root H, Rubenstein J, Boyer R, Stenroos ES, Chandrasekharappa S, Athanassiadou A, Papapetropoulos T, Johnson WG, Lazzarini AM, Duvoisin RC, Di Iorio G, Golbe LI, Nussbaum RL (1997) Mutation in the alpha-synuclein gene identified in families with Parkinson's disease. Science 276:2045–2047.

48. Recasens A, Dehay B, Bové J, Carballo-Carbajal I, Dovero S, Pérez-Villalba A, Fernagut P-O, Blesa J, Parent A, Perier C, Fariñas I, Obeso JA, Bezard E, Vila M (2014) Lewy body extracts from Parkinson disease brains trigger α-synuclein pathology and neurodegeneration in mice and monkeys. 75:351–362. doi: 10.1002/ana.24066

49. Sanders LH, Laganière J, Cooper O, Mak SK, Vu BJ, Huang YA, Paschon DE, Vangipuram M, Sundararajan R, Urnov FD, Langston JW, Gregory PD, Zhang HS, Greenamyre JT, Isacson O, Schüle B (2014) LRRK2 mutations cause mitochondrial DNA damage in iPSC-derived neural cells from Parkinson's disease patients: Reversal by gene correction. Neurobiol Dis 62:381–386. doi: 10.1016/j.nbd.2013.10.013

50. Shimozawa A, Ono M, Takahara D, Tarutani A, Imura S, Masuda-Suzukake M, Higuchi M, Yanai K, Hisanaga S-I, Hasegawa M (2017) Propagation of pathological α-synuclein in marmoset brain. Acta Neuropathol Commun 5:12. doi: 10.1186/s40478-017-0413-0

51. Singleton AB, Farrer M, Johnson J, Singleton A, Hague S, Kachergus J, Hulihan M, Peuralinna T, Dutra A, Nussbaum R, Lincoln S, Crawley A, Hanson M, Maraganore D, Adler C, Cookson MR, Muenter M, Baptista M, Miller D, Blancato J, Hardy J, Gwinn-

Hardy K (2003) alpha-Synuclein locus triplication causes Parkinson's disease. Science 302:841–841. doi: 10.1126/science.1090278

52. Steger M, Tonelli F, Ito G, Davies P, Trost M, Vetter M, Wachter S, Lorentzen E, Duddy G, Wilson S, Baptista MA, Fiske BK, Fell MJ, Morrow JA, Reith AD, Alessi DR, Mann M (2016) Phosphoproteomics reveals that Parkinson's disease kinase LRRK2 regulates a subset of Rab GTPases. Elife (Cambridge) 5:809. doi: 10.7554/eLife.12813

53. Taguchi K, Watanabe Y, Tsujimura A, Tatebe H, Miyata S, Tokuda T, Mizuno T, Tanaka M (2014) Differential expression of alpha-synuclein in hippocampal neurons. PLoS ONE 9:e89327. doi: 10.1371/journal.pone.0089327

54. Tsunemoto R, Lee S, Szűcs A, Chubukov P, Sokolova I, Blanchard JW, Eade KT, Bruggemann J, Wu C, Torkamani A, Sanna PP, Baldwin KK (2018) Diverse reprogramming codes for neuronal identity. Nature 51:987. doi: 10.1038/s41586-018-0103-5

55. Volpicelli-Daley LA, Abdelmotilib H, Liu Z, Stoyka L, Daher JPL, Milnerwood AJ, Unni VK, Hirst WD, Yue Z, Zhao HT, Fraser K, Kennedy RE, West AB (2016) G2019S-LRRK2 Expression Augments α-Synuclein Sequestration into Inclusions in Neurons. Journal of Neuroscience 36:7415–7427. doi: 10.1523/JNEUROSCI.3642-15.2016

56. Volpicelli-Daley LA, Luk KC, Lee VMY (2014) Addition of exogenous α-synuclein preformed fibrils to primary neuronal cultures to seed recruitment of endogenous α-synuclein to Lewy body and Lewy neurite-like aggregates. Nat Protoc 9:2135–2146. doi: 10.1038/nprot.2014.143

57. Volpicelli-Daley LA, Luk KC, Patel TP, Tanik SA, Riddle DM, Stieber A, Meaney DF, Trojanowski JQ, Lee VMY (2011) Exogenous α-synuclein fibrils induce Lewy body pathology leading to synaptic dysfunction and neuron death. NEURON 72:57–71. doi: 10.1016/j.neuron.2011.08.033

58. West AB, Cowell RM, Daher JPL, Moehle MS, Hinkle KM, Melrose HL, Standaert DG, Volpicelli-Daley LA (2014) Differential LRRK2 expression in the cortex, striatum, and substantia nigra in transgenic and nontransgenic rodents. J Comp Neurol 522:2465–2480. doi: 10.1002/cne.23583

59. West AB, Moore DJ, Biskup S, Bugayenko A, Smith WW, Ross CA, Dawson VL, Dawson TM (2005) Parkinson's disease-associated mutations in leucine-rich repeat kinase 2 augment kinase activity. Proc Natl Acad Sci USA 102:16842–16847. doi: 10.1073/pnas.0507360102

60. Yun SP, Kam T-I, Panicker N, Kim S, Oh Y, Park J-S, Kwon S-H, Park YJ, Karuppagounder SS, Park H, Kim S, Oh N, Kim NA, Lee S, Brahmachari S, Mao X, Lee JH, Kumar M, An D, Kang SU, Lee Y, Lee KC, Na DH, Kim D, Lee SH, Roschke VV, Liddelow SA, Mari Z, Barres BA, Dawson VL, Lee S, Dawson TM, Ko HS (2018) Block of A1 astrocyte conversion by microglia is neuroprotective in models of Parkinson's disease. Nat Med 46:957. doi: 10.1038/s41591-018-0051-5

61. Zarranz JJ, Alegre J, Gómez-Esteban JC, Lezcano E, Ros R, Ampuero I, Vidal L, Hoenicka J, Rodriguez O, Atarés B, Llorens V, Gomez Tortosa E, del Ser T, Muñoz DG, de Yebenes JG (2004) The new mutation, E46K, of alpha-synuclein causes Parkinson and Lewy body dementia. Ann Neurol 55:164–173. doi: 10.1002/ana.10795

62. Zhang Y, Chen K, Sloan SA, Bennett ML, Scholze AR, O'Keeffe S, Phatnani HP, Guarnieri P, Caneda C, Ruderisch N, Deng S, Liddelow SA, Zhang C, Daneman R, Maniatis T, Barres BA, Wu JQ (2014) An RNA-Sequencing Transcriptome and Splicing Database of Glia, Neurons, and Vascular Cells of the Cerebral Cortex. Journal of Neuroscience 34:11929–11947. doi: 10.1523/JNEUROSCI.1860-14.2014

63. Zhang Y, Pak C, Han Y, Ahlenius H, Zhang Z, Chanda S, Marro S, Patzke C, Acuna C, Covy J, Xu W, Yang N, Danko T, Chen L, Wernig M, Südhof TC (2013) Rapid single-step induction of functional neurons from human pluripotent stem cells. NEURON 78:785–798. doi: 10.1016/j.neuron.2013.05.029

64. Zhao HT, John N, Delic V, Ikeda-Lee K, Kim A, Weihofen A, Swayze EE, Kordasiewicz HB, West AB, Volpicelli-Daley LA (2017) LRRK2 Antisense Oligonucleotides Ameliorate α-Synuclein Inclusion Formation in a Parkinson's Disease Mouse Model. Mol Ther Nucleic Acids 8:508–519. doi: 10.1016/j.omtn.2017.08.002

65. Zimprich A, Biskup S, Leitner P, Lichtner P, Farrer M, Lincoln S, Kachergus J, Hulihan M, Uitti RJ, Calne DB, Stoessl AJ, Pfeiffer RF, Patenge N, Carbajal IC, Vieregge P, Asmus F, Müller-Myhsok B, Dickson DW, Meitinger T, Strom TM, Wszolek ZK, Gasser T (2004) Mutations in LRRK2 cause autosomal-dominant parkinsonism with pleomorphic pathology. NEURON 44:601–607. doi: 10.1016/j.neuron.2004.11.005

Figure Legends – Main Figures

Figure 1: PFF-based screen in primary neuron identifies Lrrk2 and Gba as genetic modifiers of α-synuclein transmission and aggregation.
(a) Schematic of experimental design: lentiviral knock-down or overexpression of Parkinson's disease (PD) risk genes in primary neuron cultures exposed to sonicated α-syn preformed fibrils (PFFs) at 10 days in vitro (DIV). Survival and aggregation of endogenously expressed α-syn was measured using immunolabeling of phosphorylation of α-syn at Serine 129 (pSer129) 10 days after PFF treatment. **(b,c)** Representative images **(b)** and quantification of pSer129-positive (green) α-syn aggregation **(c)** following knock down of Snca, Gba, Lrrk2 and non-targeting scramble (SCR) control (n=8-10 independent wells/treatment). pSer129 immunolabeling was normalized to neuron counts using the neuronal marker NeuN (red). A minimum of 2 shRNAs with a KD-efficiency of 50 percent were used per PD risk gene. **(d,e)** Experimental design **(d)** and quantification of PFF-based α-syn aggregation **(e)** in primary neuron cultures derived from LRRK2 G2019S-mutant (G2019S) and WT mouse embryos (n=10 wells/genotype, 10 images/well). **(f)** Relative α-syn (Snca) mRNA expression level measured in WT and G2019S-LRRK2 mutant neurons at 10DIV using quantitative RT-qPCR analysis (n=5/group). Data expressed as mean + SEM; *$p < 0.05$; **p

< 0.01; compared by unpaired Student's t-test and one-way ANOVA with a Tukey's post-test for multiple comparisons.

Figure 2: The LRRK2 G2019S mutation exacerbates α-syn pathology in a PFF-based mouse model of α-syn transmission and aggregation *in vivo*.
(a,b) Schematic of mouse genotypes and experimental design. Adult LRRK2 G2019S BAC-transgenic mice (G2019S or GS) and wildtype (WT) littermates were injected with α-syn PFFs or vehicle control. Histological analysis and behavioral testing was performed at 1,3,6 months post injection (PI). **(c)** Representative images of pSer129 (green) immune-labeling in TH-positive neurons (red) in the substantia nigra pars compacta (SNpc) at 6 months PI. **(d)** Quantification of the percentage of TH-positive neurons that are also pSer129-positive in the SNpc of PFF-injected animals (n=8-13 animals/group, 8-10 brain sections/animal). **(e)** Quantification of the number of TH-positive neurons in the SNpc of WT and LRRK2-G2019S animals at 1,3,6 months post injection with PFFs or vehicle control (n=6-12 animals/group, 8-10 brain sections/animal). **(f)** Schematic and results of open field behavioral testing 6 months post injection with PFFs or vehicle control (11-13 animal/group). **(g)** Rotarod behavioral assay measuring the latency to fall from an accelerating rotating cylinder at 6 months post injection (n=11-13 animals/group). Data expressed as mean + SEM; *p < 0.05; compared by Student's t-test and one-way ANOVA with a Tukey's post-test for multiple comparisons.

Figure 3: Recombinant human α-syn PFFs induce aggregation of endogenous α-syn in human iPS-derived induced neurons.
(a) Experimental design: iPS-derived iNs were differentiated for 3 weeks before the addition of 1uM of human α-syn PFFs to the culture media. Aggregation of endogenously expressed α-syn was assessed using immunolabeling of pSer129. **(b,c)** Representative images **(b)** and quantification **(c)** of pSer129 immunolabeling (red) up to 14 days post PFF treatment (n=19-21 frames/time point). Nuclei labeled with DAPI (blue). **(d)** Representative images of pSer129 α-syn (red) co-localizing with the axonal marker BIII-tubulin (magenta) 7 days post PFF treatment. **(e)** Representative images of pSer129 α-syn (red) co-localizing with ubiquitin (green) 14 days post PFF treatment. Data expressed as mean + SEM; compared by one-way ANOVA with a Tukey's post-test for multiple comparisons.

Figure 4: LRRK2 modulates aggregation of α-syn in human induced neurons (iNs).
(a) Experimental design of internalization of α-syn PFFs. 3 week old iNs were exposed to fluorescently labeled α-syn PFFs for 0 to 24 hours. Fluorescence in the media was quenched with 0.1% Trypan blue, revealing the internalized labeled PFFs. **(b)** Representative image of internalized PFFs (green) in human iNs (brightfield) after 6 hours of incubation. **(c)** Quantification of internalized PFFs in isogenic G2019S mutant, corrected and knock out (KO) iNs after 1-24 hours of incubation (n=300-450 cells from two biological replicates/condition). Data expressed as mean + SD, compared by two-way ANOVA with Bonferroni post hoc correction. **(d,e)** Representative images and quantification of pSer129-positive α-syn aggregates after 3 weeks of incubation with recombinant human PFFs (n=10-12wells/group). Data expressed as mean + SEM; *p < 0.05; **p < 0.01; compared by one-way ANOVA with a Tukey's post-test for multiple comparisons. **(f)** Representative Western blot of isogenic LRRK2 G2019S mutant, corrected and knock out (KO) iN lysates 2 weeks post PFF treatment, probed with anti-pSer129, anti-PSD95, anti-SYNAPTOPHYSIN (SYP) and anti-ACTB antibodies. Synaptic proteins and ACTB were used as loading controls. Proteins were sequentially extracted using 1% Triton-X followed by 2% SDS lysis buffers. **(g-h)** Quantification of pSer129 **(g)**, PSD95 **(h)** and SYNAPTOPHYSIN **(i)** 14

days post PFF treatment (n = 4/group). Data expressed as mean + SEM; *p < 0.05; **p<0.01; compared by one-way ANOVA with a Tukey's post-test for multiple comparisons.

Figure 5: Impaired α-syn expression in LRRK2 knock out iNs.
(a) Representative Western blot of isogenic LRRK2 G2019S mutant, corrected and knock out (KO) iNs at 4 weeks of differentiation probed with anti-LRRK2, anti-α-syn (SNCA), anti-PSD95, anti-SYNAPTOPHYSIN (SYP), anti-HOMER1 and anti-ACTB antibodies. ACTB was used as a loading control. **(b-e)** Quantification of α-syn (**f**), PSD-95 (**g**), SYNAPTOPHYSIN (SYP) **(d)** and HOMER1 level at 4 weeks of differentiation (n=3/group). Data expressed as mean + SD; compared by one-way ANOVA with a Tukey's post-test for multiple comparisons. **(f-i)** qRT-PCR expression analysis of mature neuron markers MAP2 **(f)**, MAPT **(g)** and synaptic markers SNAP25 **(h)** and GRIA1 **(i)** during 4 weeks of differentiation. Data normalized to the 0 weeks of differentiation time point (n=4/group and time point). Data expressed as mean + SEM; *p < 0.05; **p<0.01; compared by one-way ANOVA with a Tukey's post-test for multiple comparisons and two-way ANOVA with Bonferroni post hoc correction.

Figure 6: PFF-based α-syn transmission and aggregation is exacerbated by the LRRK2 across models.
Schematic of the neuron-to-neuron transmission of α-syn pathology. α-syn aggregates are transported along axons, released and internalized by other neurons, where they can trigger aggregation of endogenous α-syn. Degenerative phenotypes are associated with glial activation and behavioral impairments.

Bieri_Figure 1

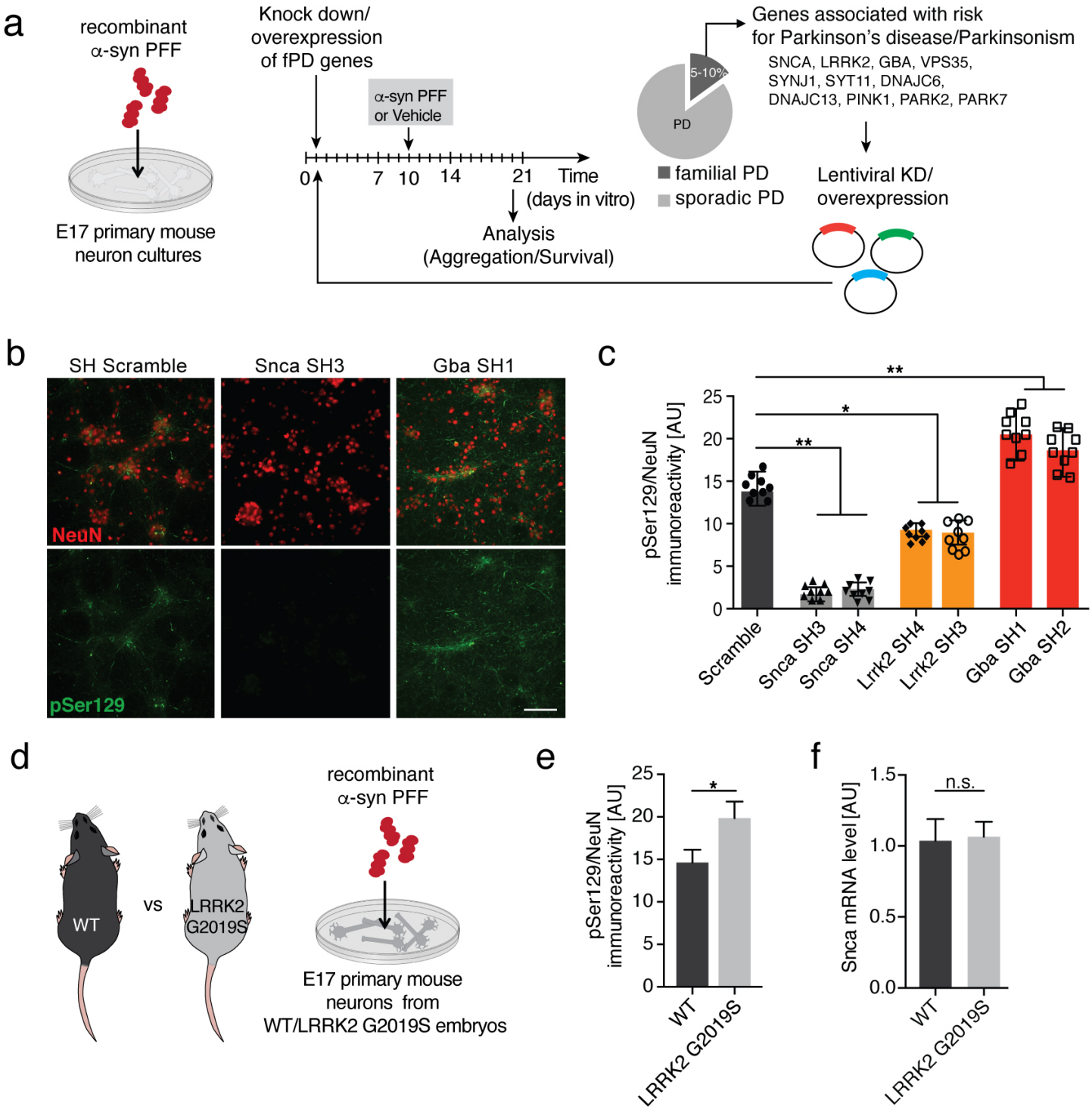

Bieri_Figure 2

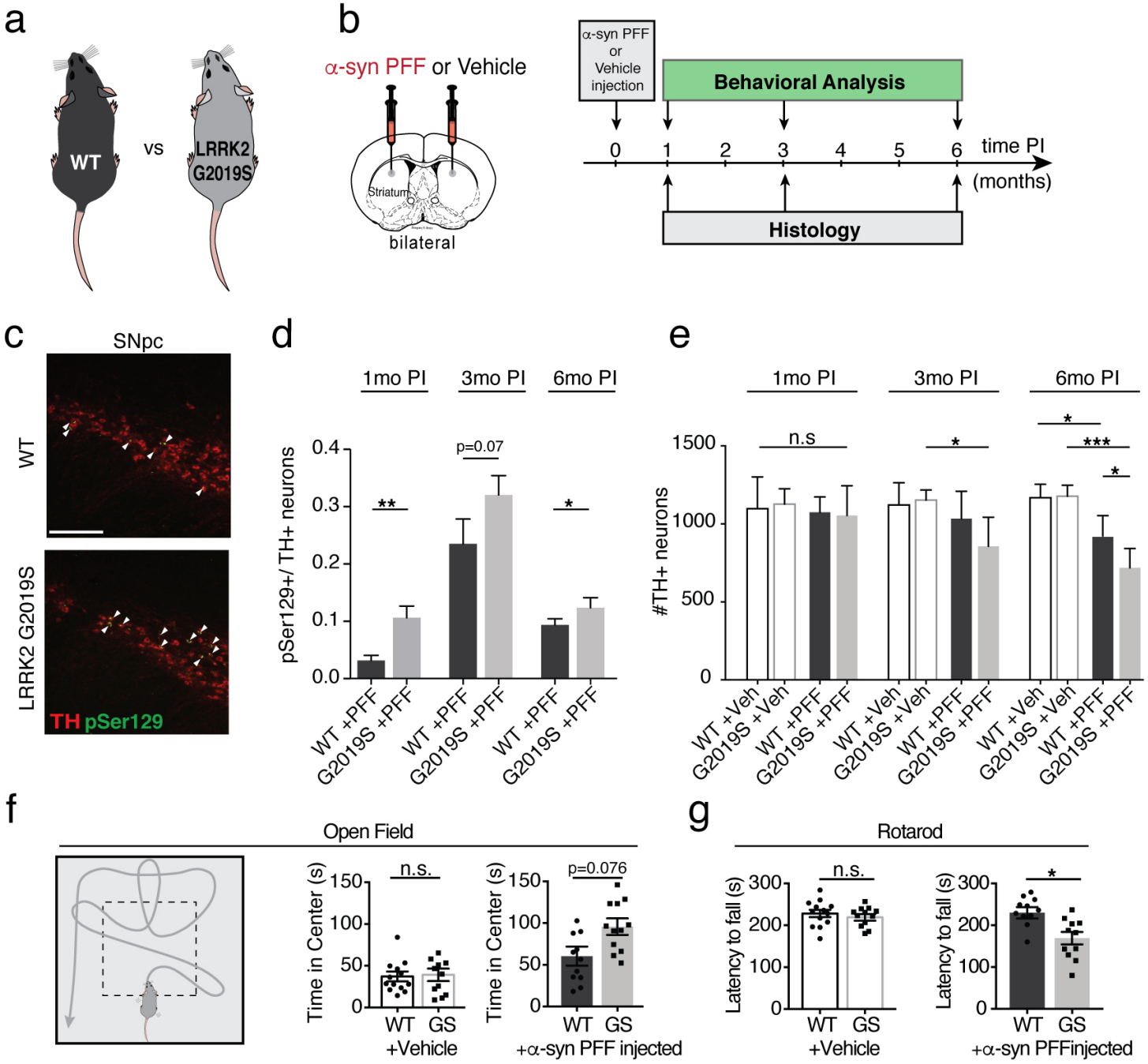

Bieri_Figure 3

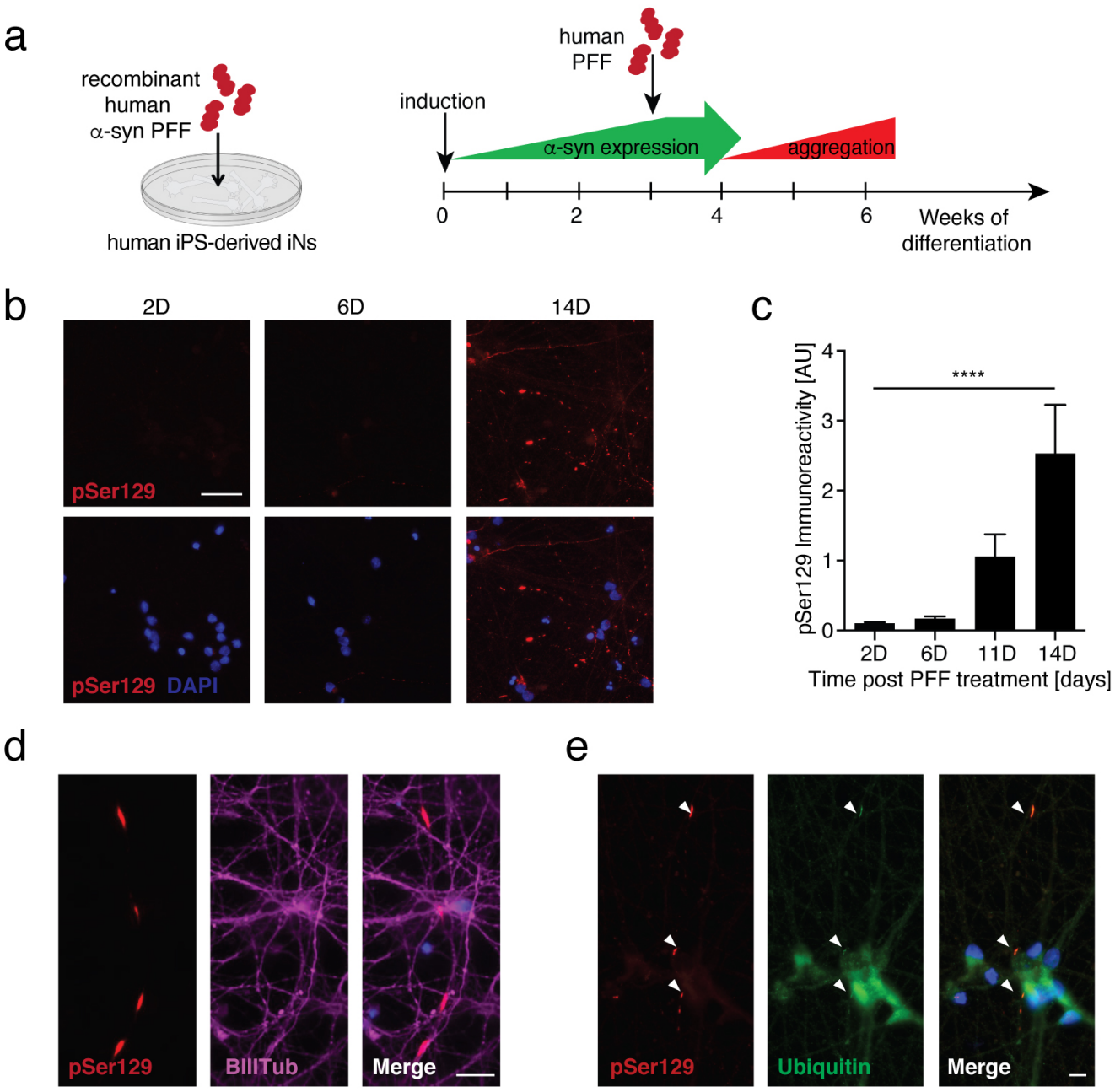

Bieri_Figure 4

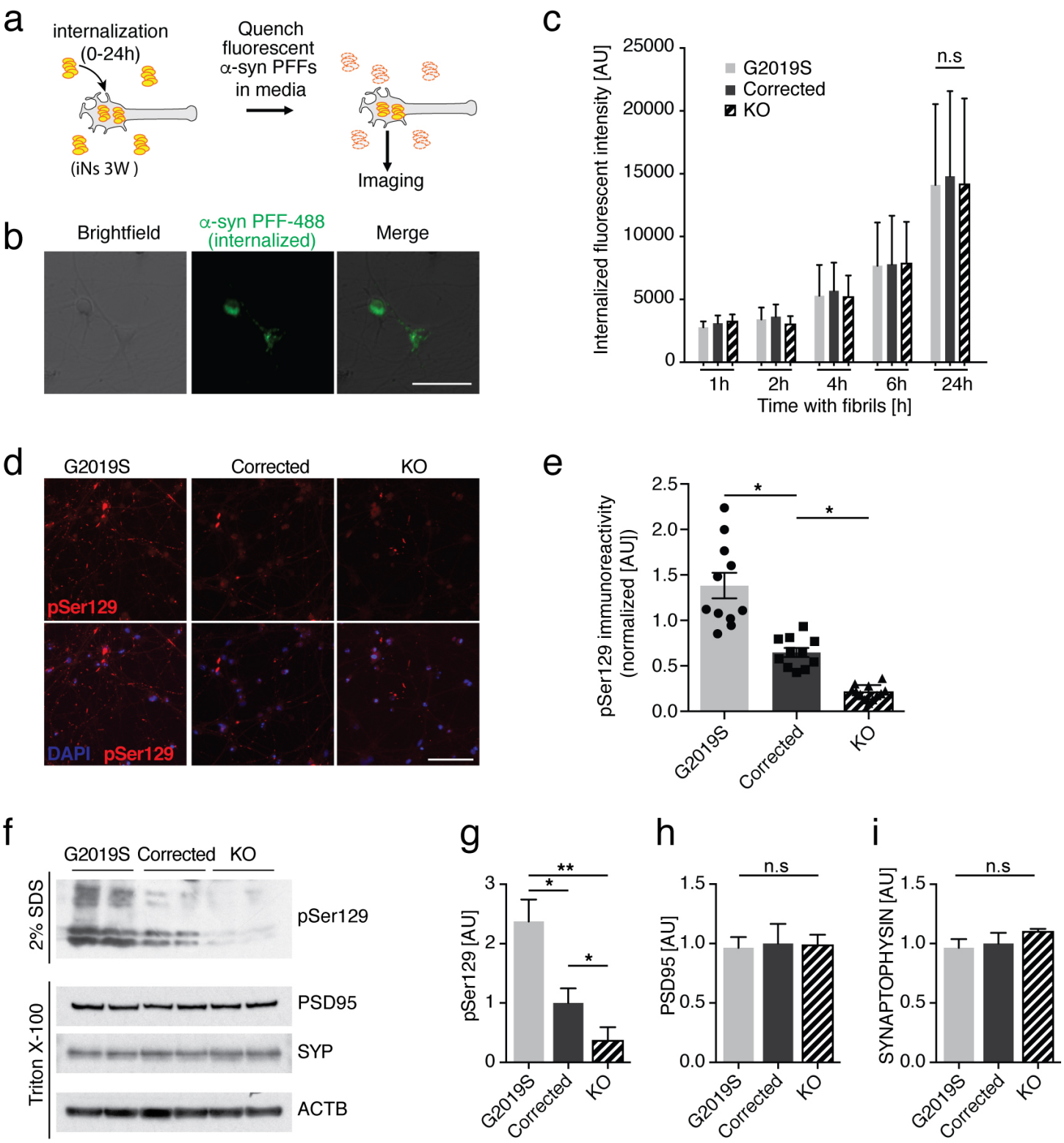

Bieri_Figure 5:

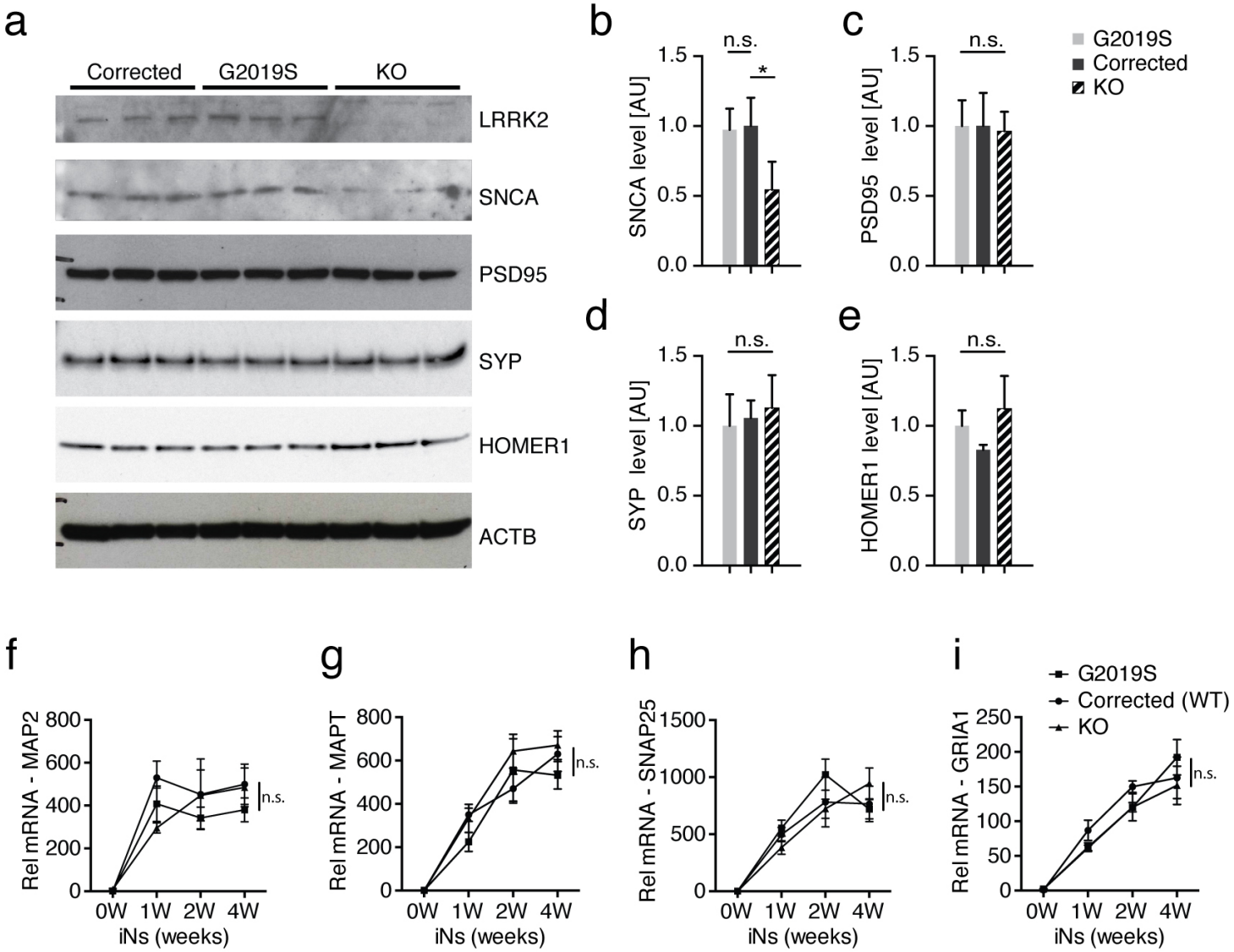

Bieri_Figure 6

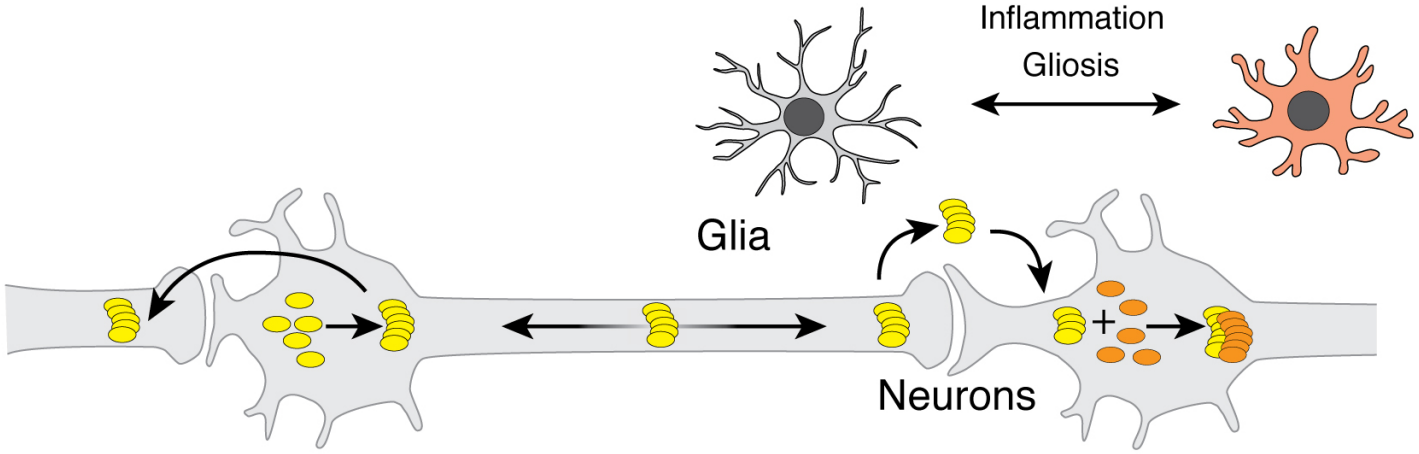

Supplementary Material

Figure Legends – Supplementary Figures

Figure S1: Recombinant α-syn PFFs induce aggregation of endogenous α-syn in primary neurons *in vitro.*
(a) Electron microscopy image of recombinant mouse α-syn fibrils. **(b)** Schematic of lentiviral or PFF-based α-syn aggregation assay. Primary cortical neurons from E17 mouse embryos were infected with α-syn expressing lentivirus or treated with 0.5ug/ml sonicated mouse α-syn PFFs at 10 days in vitro (DIV). Neuronal survival and pSer129-α-syn aggregation was measured 1, 3, 6, 10 days post PFF/lentiviral treatment. **(c,d)** Neuronal survival was measured using luminescence-based LDH activity assays **(c)** and CaspaseGlo DEVDase assays **(d)** 10 days after lentiviral infection or PFF addition to the culture media. **(e,f)** Representative images **(c)** and quantification **(d)** of pSer129-α-syn aggregation (green) 3-10 days post PFF treatment. MAP2 (magenta) was used as a marker for neuronal processes (n=8 wells/time point). Data expressed as mean + SEM; *$p < 0.05$; **$p < 0.01$; ***$p < 0.001$; compared by one-way ANOVA with a Tukey's post-test for multiple comparisons.

Figure S2: Targeted Lentiviral knockdown and overexpression screen in primary neurons.
(a-f) Lentivirus-mediated knock-down efficiency was measured using quantitative RT-PCR analysis. Neurons were infected on 1 day in vitro (DIV) and mRNA was isolated on 10 DIV. 4-5 different shRNA constructs were generated per Parkinson's disease risk gene. Representative knock down efficiency of shRNAs targeting Lrrk2 **(a)**, Gba **(b)**, Snca **(c)**, non-targeting scramble control **(d)**, Pink1 **(e)** and Park2 **(f)**, normalized to Scramble control (n=3-4 wells/shRNA). **(g)** Representative column bar graph indicating the normalized α-syn pSer129 aggregation score for all shRNA and overexpression conditions. Neuronal viability was determined by the number of NeuN-positive cells/well in PFF compared to vehicle treated wells. The aggregation score was calculated based on pSer129 immunolabeling and normalized to the neuronal viability for each shRNA and scramble shRNAs. The dotted line marks the average of all non-targeting scramble shRNAs. α-syn (Snca) constructs are indicated in yellow, Lrrk2 in red, scramble in gray and Gba in blue. Samples are arrange from smallest to largest amount of relative pSer129 immunolabeling using the standardized PFF-based transmission and aggregation screening assay (n=12-24 wells/shRNA). Data expressed as mean + SEM; *$p < 0.05$; **$p < 0.01$;****$p<0.0001$ compared by one-way ANOVA with a Tukey's post-test for multiple comparisons.

Figure S3: Characterization and manipulation of Gba and Lrrk2 in primary neurons *in vitro.*
(a,b) Representative Western blot **(a)** and quantifications **(b)** of lysates from primary neurons infected with Gba and non-targeting scramble shRNAs (SCR), collected 9 days post infection. Blots were probed with anti-α-syn, anti-ActB and anti-Gba antibodies. ActB was used as a loading control and the data normalized to the scramble condition (n=4/group). Data expressed as mean + SD. **(c)** Schematic of experimental design: Primary neurons were isolated from CAG-Cas9 transgenic E17 embryos, infected with Lrrk2 and non-targeting (NT) gRNAs on 1 DIV and treated with sonicated α-syn PFF at 10DIV. **(d)** α-syn aggregation and viability was measured using pSer129 and NeuN immunolabeling 10 days post fibril treatment (n=10 wells/group). **(e)** Relative α-syn (Snca) mRNA expression level measured in NT and Lrrkt gRNA infected neurons at 10DIV using quantitative RT-PCR analysis. Data was normalized to the NT condition (n=6 wells/group) **(f)** Representative Sanger sequencing chromatogram of the G to A nucleotide mutation in exon 41

of the human LRRK2 in the BAC transgenic mouse line. Mutation marked in red. **(g,h)** Relative mRNA expression level of the synaptic markers Synaptophysin **(g)** and Snap25 **(h)** in WT compared to LRRK2 G2019S transgenic primary neurons at 10 DIV (n=6 wells/group). **(i,j)** Neuronal survival of α-syn PFF and Vehicle (Veh) treated WT compared to LRRK2-G2019S primary neurons was measured using LDH **(i)** and CaspaseGlo **(j)** activity assays (n=12 wells/group). **k** Quantification of internalization in G2019S LRRK2 and WT primary neuron cultures after 1-24 hours of incubation with fluorescently labeled sonicated α-syn PFFs (n=4 wells, 112-145 cells/well). Data expressed as mean + SEM; *$p < 0.05$; compared by unpaired Student's t-test and one-way ANOVA with a Tukey's post-test for multiple comparisons and two-way ANOVA with Bonferroni post hoc correction.

Figure S4: Characterization of histological and behavioral phenotypes in α-syn PFF-injected wild-type mice.
(a) Experimental design: adult wildtype (WT) mice were stereotaxically injected with recombinant mouse α-syn PFFs or vehicle control (Veh) into the dorsal striatum, followed by behavioral testing and histological analysis up to 6 months post injection (PI). **(b)** Representative images of pSer129-postive (green) and p62-positive (red) α-syn aggregates and DAPI (blue) in the dorsal striatum. **(c)** Representative images of pSer129-postive aggregates (green) in TH-positive (red) dopaminergic neurons in the SNpc 2 months PI. Quantification of percentage of TH-positive neurons with pSer129-positive inclusions (n=8-12 animals/group). **(d)** Representative images of TH-positive (red) dopaminergic neurons in SNpc ipsilateral and contralateral to the injection site at 2 and 6 months post injection with PFFs. **(e-f)** Quantification of TH-positive neurons in in the SNpc of PFF **(e)** and vehicle control **(f)** injected animals (n=6-12 animals/group, 8-10 sections/animal). Black bars indicated the number of TH-positive neurons ipsilateral to the injection site, gray bars contralateral to the injection site. Data expressed as mean + SD. **(g-i)** Behavioral testing of PFF and vehicle control injected mice up to 6 months post injection. **(g)** Rotarod test measured the latency to fall from an accelerating rotating cylinder (n=10-12 animals/group). **(h)** Open field measures anxiety using the time spent in the center and the overall distance travelled (n=10-12 animals/group). Data expressed as mean + SEM; *$p < 0.05$; compared by Student's t-test, one-way ANOVA with a Tukey's post-test for multiple comparisons or two-way ANOVA with Bonferroni post hoc correction.

Figure S5: Characterization of G2019S LRRK2 BAC transgenic mice
(a) Schematic of mouse genotypes. **(b)** Representative Western blot of striatal brain lysates from LRRK2 G2019S-BAC transgenic (G2019S or GS) mice and WT littermate controls were probed with anti-human LRRK2, anti-α-syn and anti-ActB antibodies. ActB was used as loading control. **(c)** Quantification α-syn protein level in G2019S-LRRK2 BAC transgenic mice and WT littermate controls (n=4 animals/group). **(d)** qRT-PCR expression analysis of α-syn mRNA level in 2 months old G2019S-LRRK2 BAC transgenic mice and WT littermate controls (n=4 animals/group). **(e)** Rotarod behavioral assay measuring the latency to fall from an accelerating rotating cylinder for 2, 6, 12 months old G2019S-LRRK2 BAC transgenic mice and WT littermate controls (n=12-15/group). **(f)** Body weight measurements of 2 to 12 months old G2019S-LRRK2 BAC transgenic mice and WT littermate controls (n=20-25/group). Data expressed as mean + SEM or mean + SD; n.s.,$p > 0.05$; compared by Student's t-test, one-way ANOVA with a Tukey's post-test for multiple comparisons and two-way ANOVA with Bonferroni post hoc correction.

Figure S6: Characterization of neuroinflammatory phenotypes in LRRK2-mutant and WT PFF-injected mice.

(a) Schematic of analyzed brain area. The gray box indicates the part of the dorsal striatum used for quantifications. **(b)** Schematic of microglial morphology. **(c,d)** Representative images **(c)** and quantification **(d)** of microglial marker Iba1 (red) and pSer129 (green) in the dorsal striatum of LRRK2 G2019S (G2019S or GS) mice and WT littermate controls 6 months post-injection (PI) with PFFs or Vehicle (Veh) control (n=6-12 animals/group). **(e-g)** Experimental design and quantification of gene expression of microglial **(f)** and astrocyte-associated **(g)** activation markers. mRNA was isolated from the striatum and gene expression was analyzed using RT-qPCR analysis (n=5-6 animals/group). **(h-i)** Representative images **(h)** and quantification **(i)** of intensity of C1q immunolabeling in the dorsal striatum of PFF and vehicle injected mice 6 months post injection (n=5-6 animals/group). Data expressed as mean + SEM; *$p < 0.05$, **$p < 0.01$; compared by Student's t-test, one-way ANOVA with a Tukey's post-test for multiple comparisons or and two-way ANOVA with Bonferroni post hoc correction.

Figure S7: Rapid differentiation and upregulation of synaptic and mature neuron markers using a Ngn2-based induced neuron approach. (a) Bright field images of undifferentiated iPS colonies and induced neurons (iNs) after two weeks of differentiation *in vitro*. Schematic and time-line of Ngn2-based differentiation protocol. iPS cells differentiate rapidly into iNs following Ngn2 expression and transition into neuronal differentiation media. **(b,c)** Representative images of iNs expressing neuronal markers B-III-tubulin **(b)** and MAP2 **(c)**. **(d)** qRT-PCR analysis of human endogenous α-syn (SNCA) mRNA expression in iPS control lines during 4 weeks of iN differentiation (n=4 iPS lines/time point). Data normalized to 0 weeks of differentiation. (**e**) Representative Western blot of lysates form iNs up to 4 week of differentiation probed with anti-α-Syn and anti-ACTB antibodies. ACTB was used as a loading control. **(f-i)** qRT-PCR expression analysis of mature neuron markers MAP2 **(f)** MAPT **(g)** and synaptic markers SNAP25 **(h)** and GRIA1 **(i)** during 4 weeks of iN differentiation (n=4 iPS lines/time point). Data normalized to the 0 weeks of differentiation time point. Data expressed as mean + SEM.

Figure S8: Survival analysis of PD-patient derived isogenic LRRK2 G2019S and knock-out iNs.
(a) Representative Sanger sequencing chromatogram of the G to A nucleotide mutation in exon 1 of LRRK2 in G2019S LRRK2 mutant (top) and healthy control (bottom) iPS lines. **(c,d)** Neuronal survival of isogenic G2019S LRRK2 mutant (G2019S), corrected and knock-out (KO) iNs was measured after 4 weeks of differentiation using LDH **(b)** and CaspaseGlo DEVDase **(c)** luminescence-based activity assays (n=12 wells/line). Data expressed as mean + SD; n.s.,$p>0.05$; compared by one-way ANOVA with a Tukey's post-test for multiple comparisons.

Bieri_Figure S1

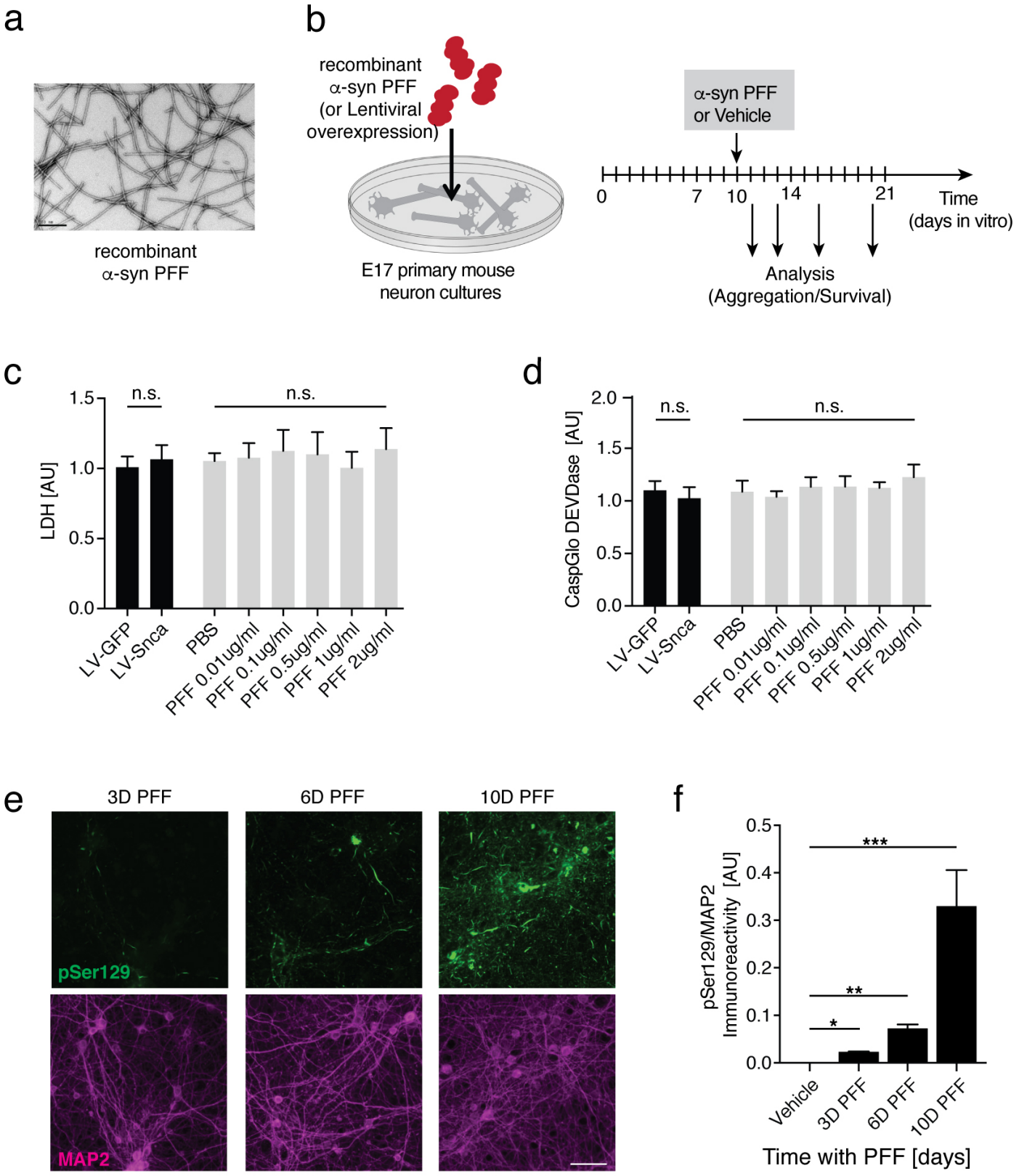

Bieri_Figure S2

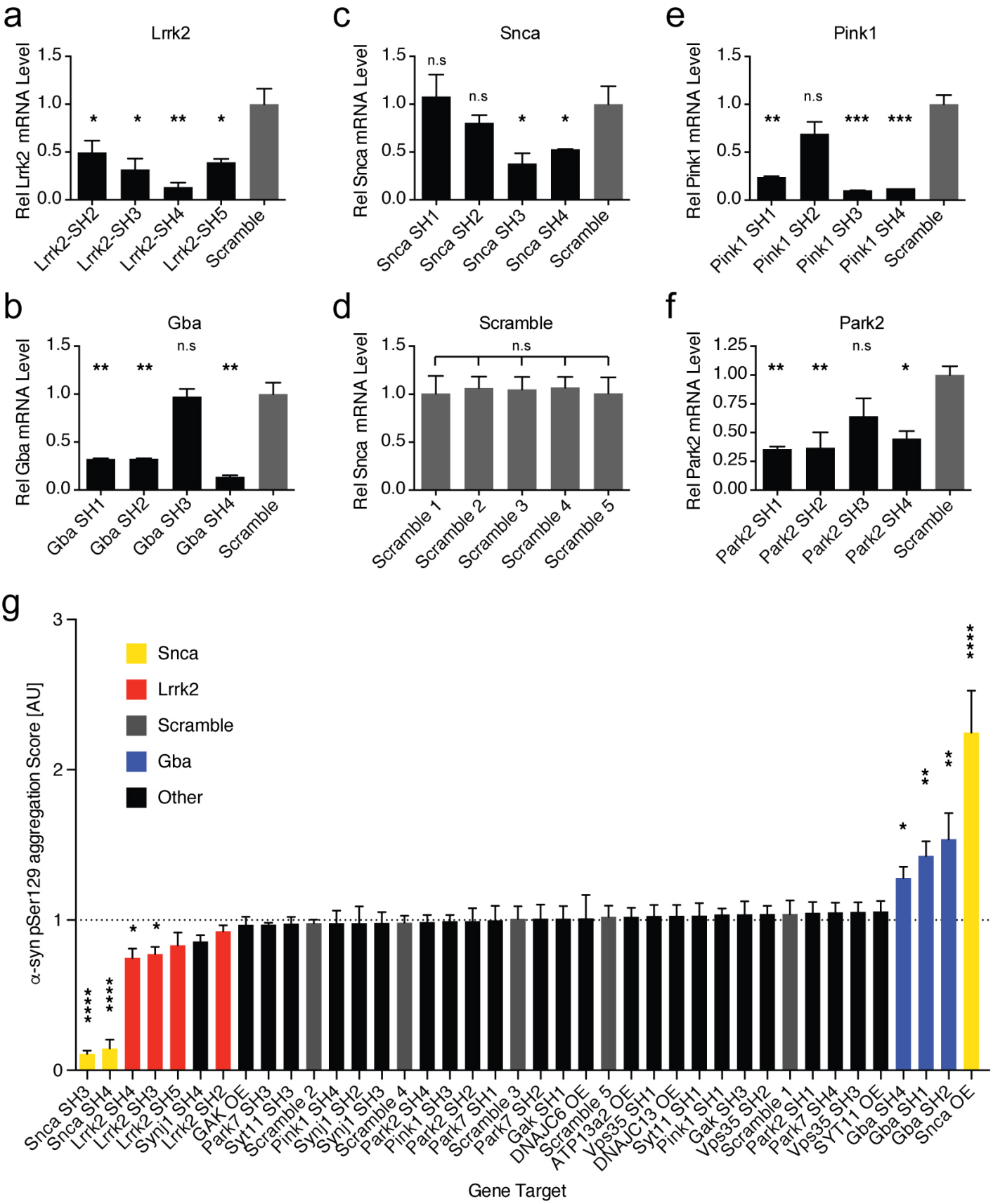

Bieri_Figure S3

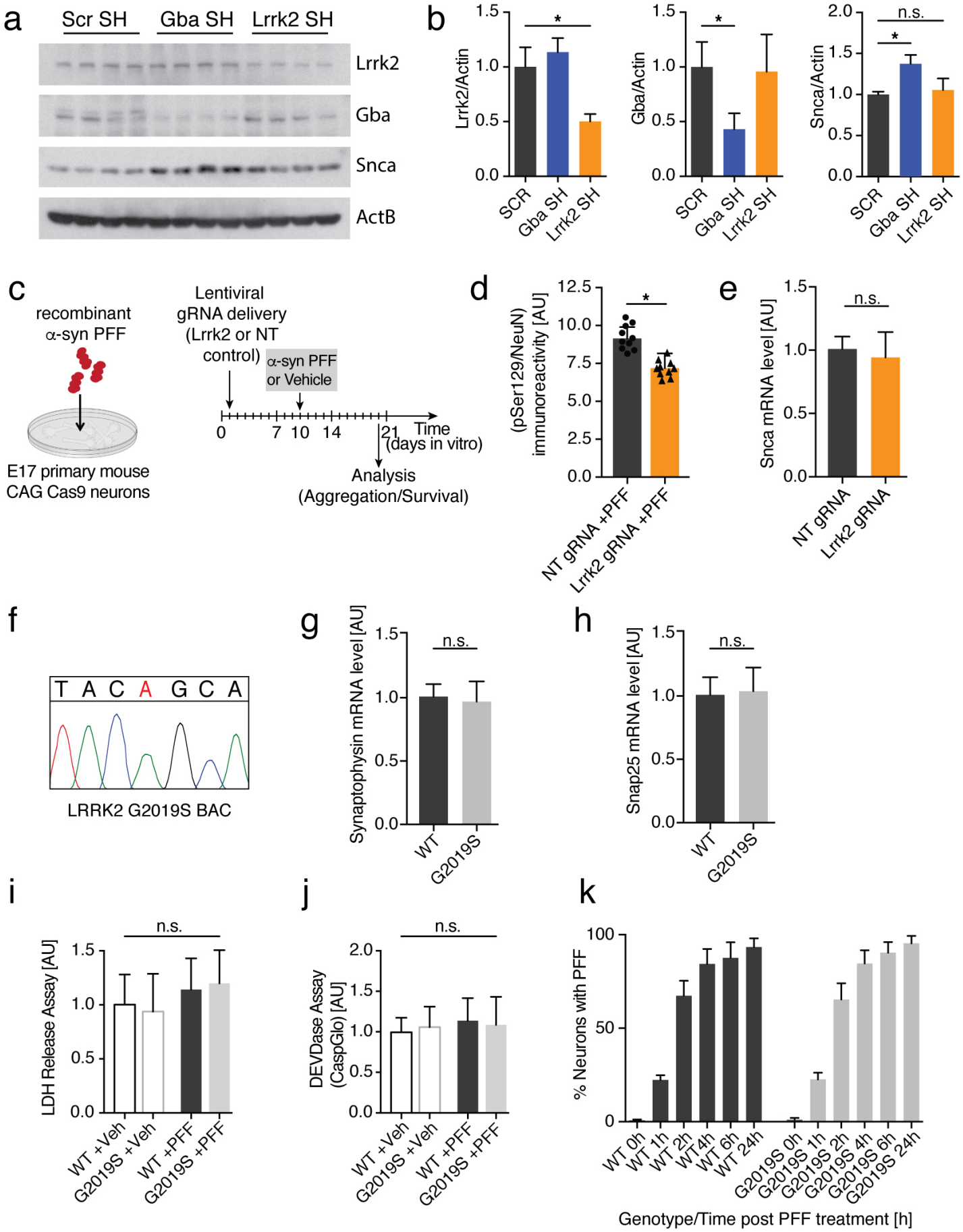

Bieri_Figure S4

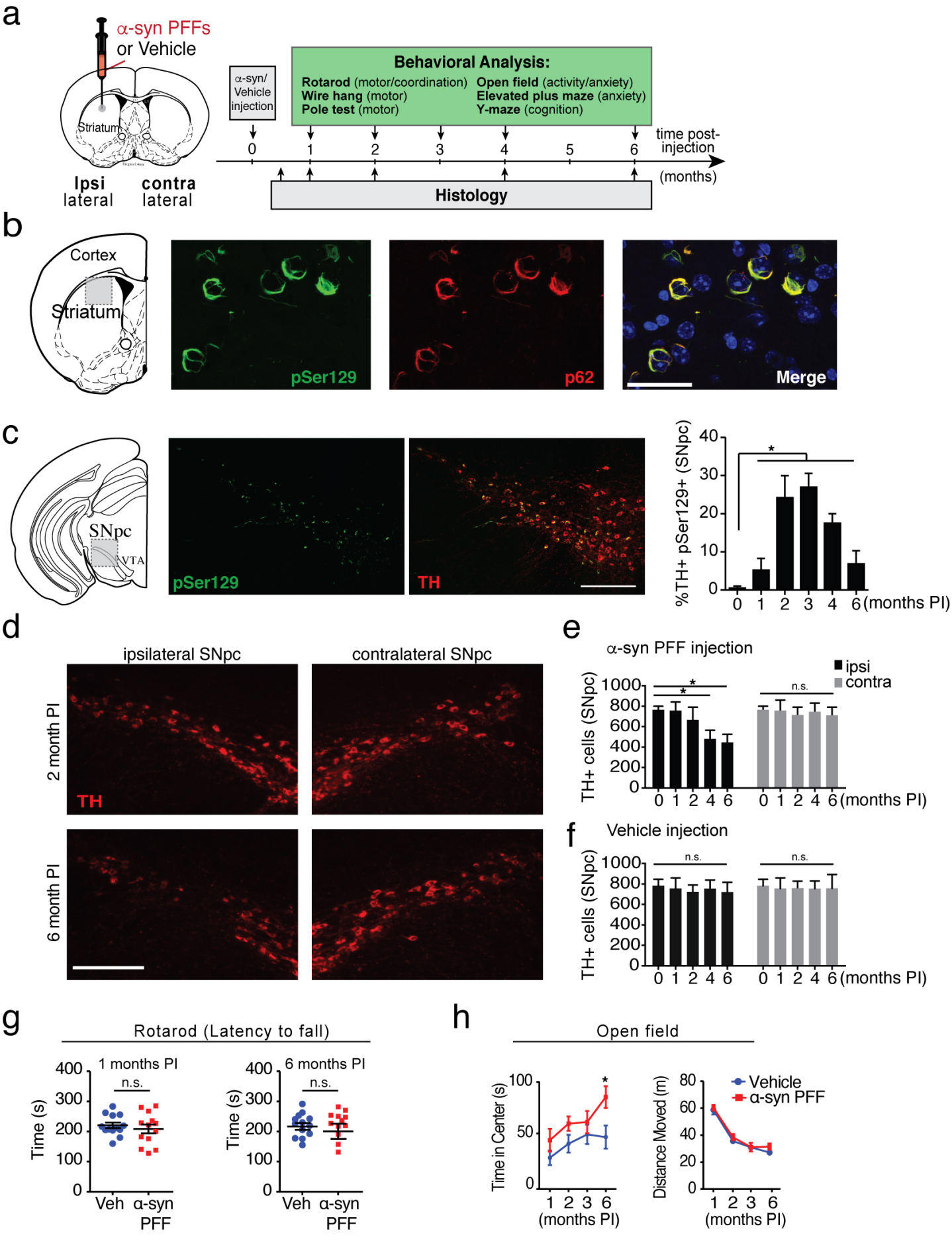

Bieri_Figure S5

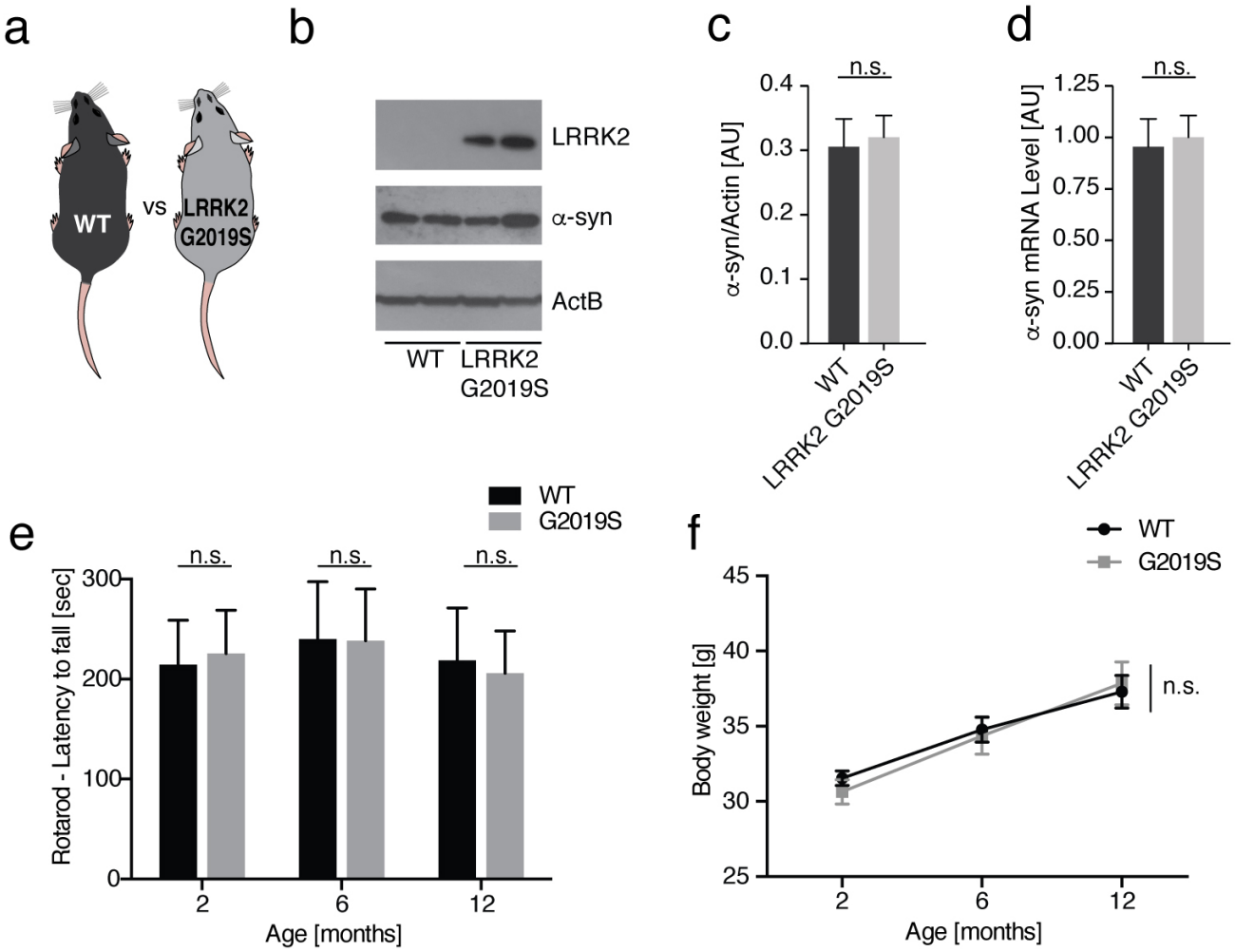

Bieri_Figure S6

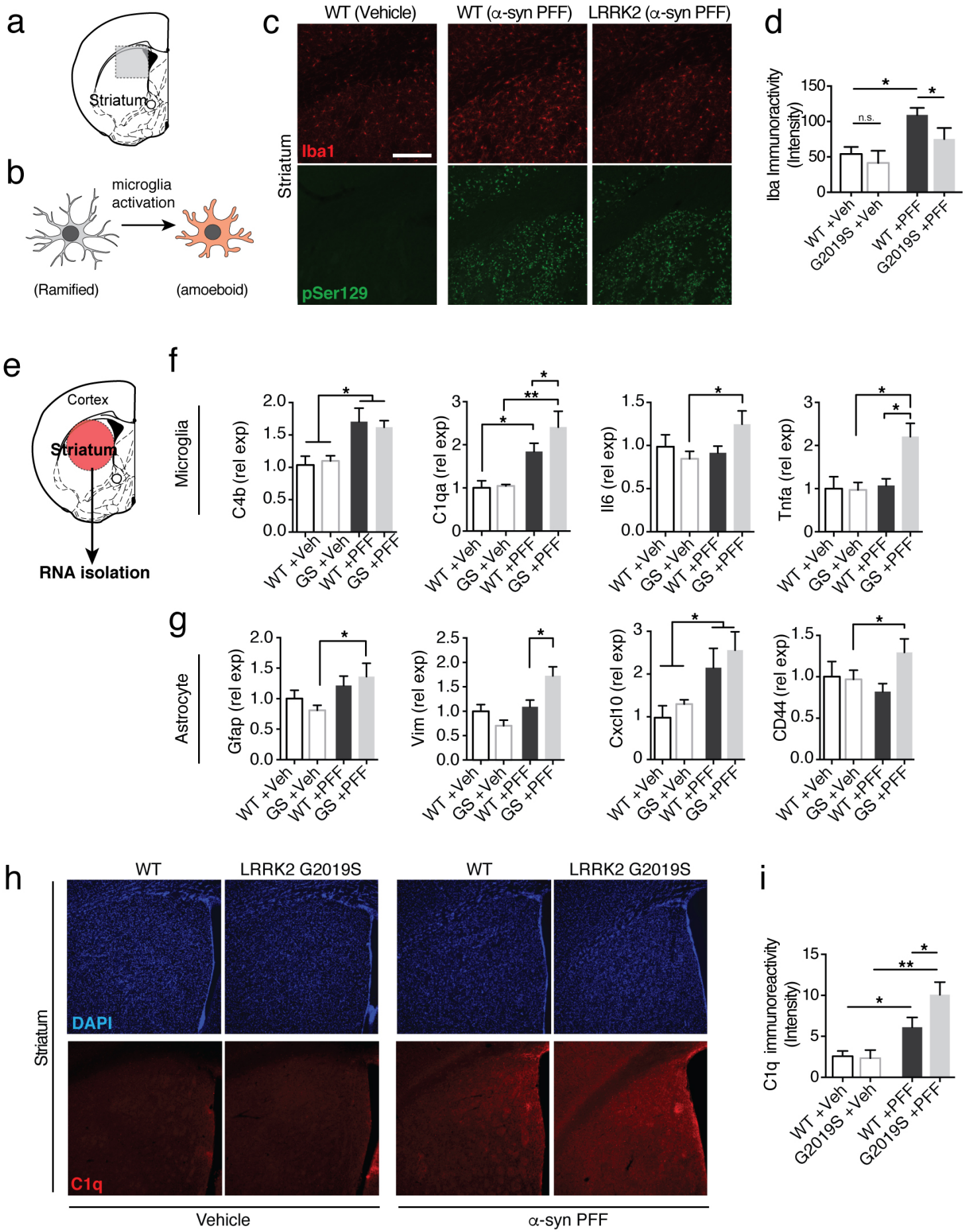

Bieri_Figure S7

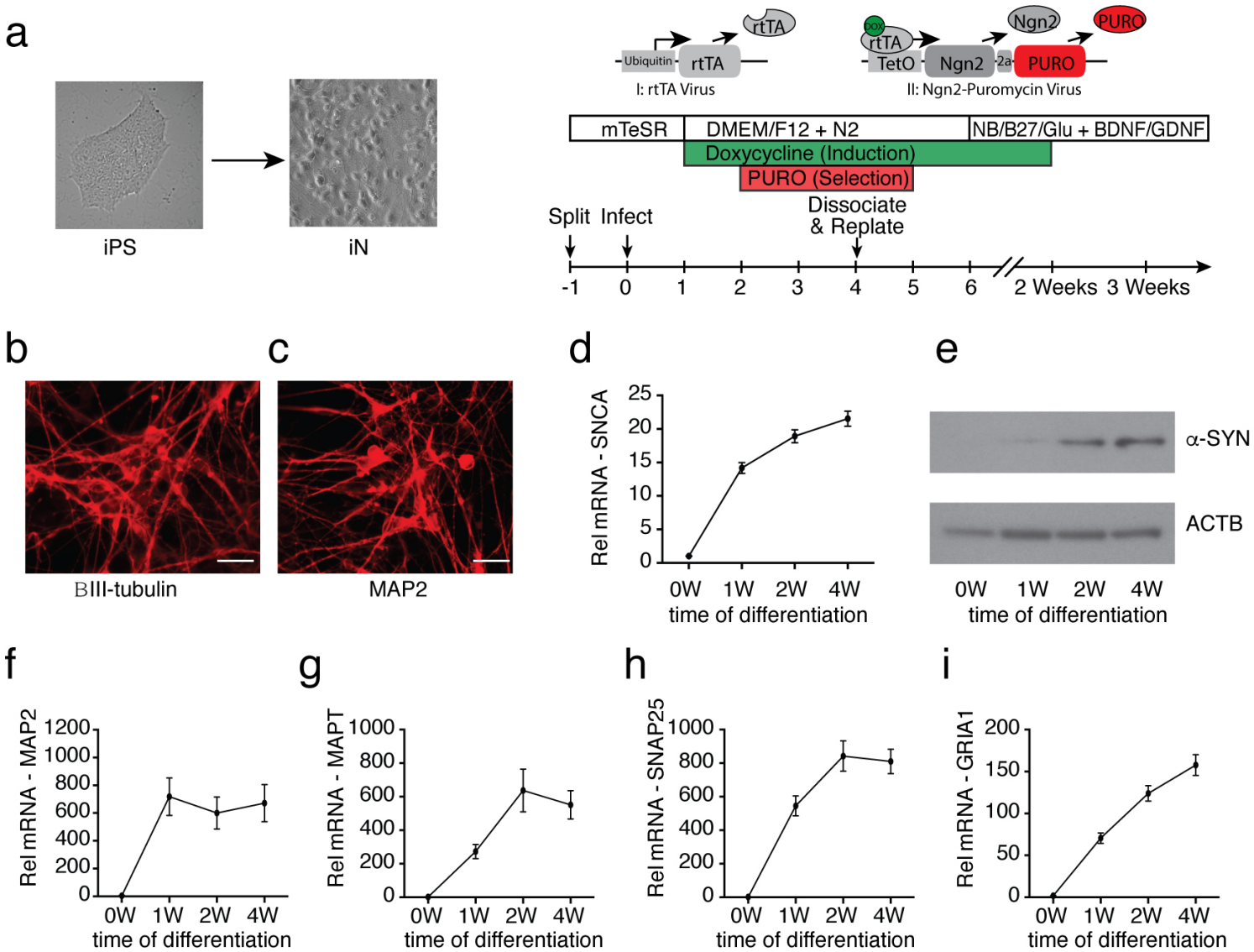
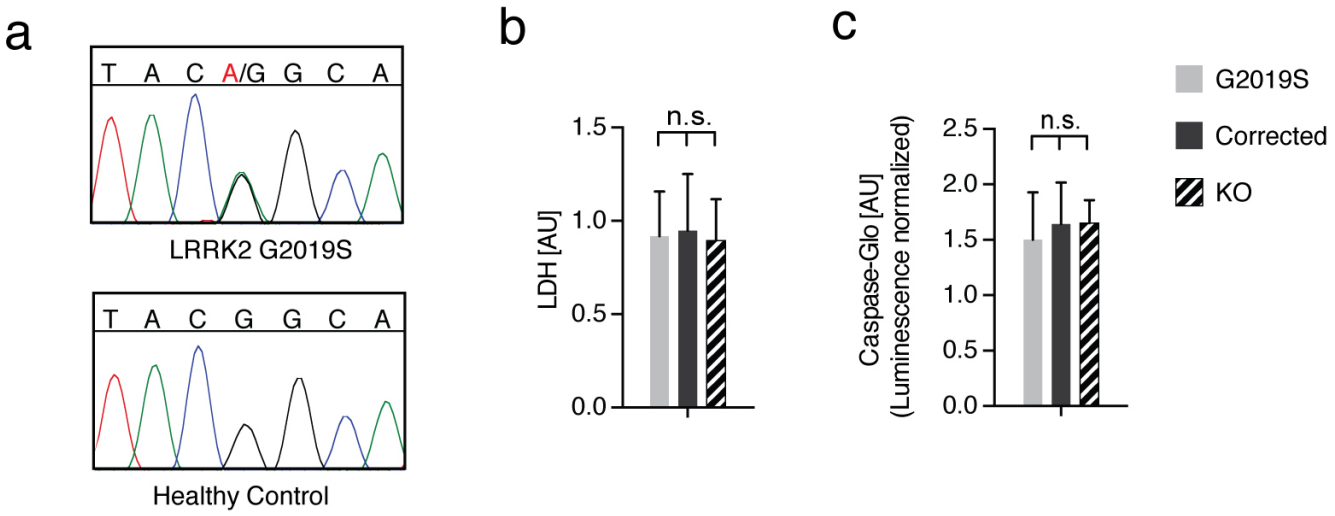
Bieri_Figure S8